Cell Stem Cell

Article

Human conjunctiva organoids to study ocular surface homeostasis and disease

Graphical abstract

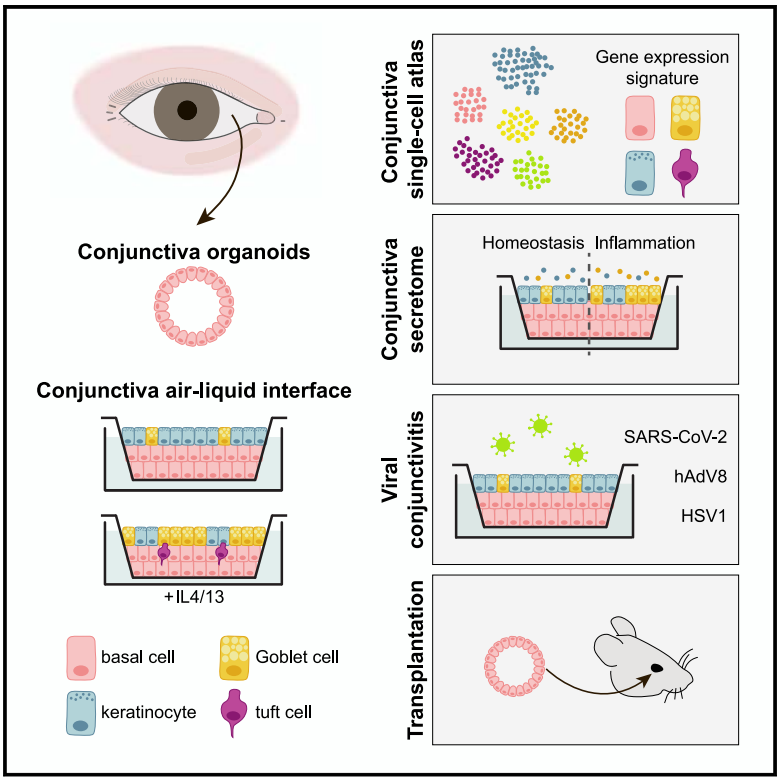

Authors

Marie Bannier-Hélaouët, Jeroen Korving, Ziliang Ma, ..., Bart L. Haagmans, Wei Wu, Hans Clevers

Correspondence

m.bannier@hubrecht.eu (M.B.-H.), h.clevers@hubrecht.eu (H.C.)

In brief

Bannier-Hélaouët and colleagues use organoids and air-liquid interfaces to study the functions of the conjunctival epithelium. Besides mucus-producing goblet cells, the conjunctival epithelium contains interleukin-responsive tuft cells and antimicrobial peptides-producing keratinocytes. Conjunctival organoids are tools to model viral conjunctivitis and could be stem cell reservoirs for ocular surface cell therapy.

Highlights

- Adult stem cell-derived conjunctiva organoids and air-liquid interface
- IL-4 and IL-13 promote conjunctiva goblet and tuft cell differentiation
- Transcriptome and secretome analysis of the conjunctival epithelium
- Orthotopic engraftment of conjunctiva organoids

Bannier-Hélaouët et al., 2024, Cell Stem Cell *31*, 227–243
February 1, 2024
https://doi.org/10.1016/j.stem.2023.12.008

CellPress

Cell Stem Cell

CellPress
OPEN ACCESS

Article

Human conjunctiva organoids to study ocular surface homeostasis and disease

Marie Bannier-Hélaouët,[1,2,*] Jeroen Korving,[1,19] Ziliang Ma,[3,19] Harry Begthel,[1,2,19] Amir Giladi,[1,2,19] Mart M. Lamers,[4,19] Willine J. van de Wetering,[5] Nobuyo Yawata,[6,7,8] Makoto Yawata,[9,10,11,12,13,14] Vanessa L.S. LaPointe,[15] Mor M. Dickman,[15,16] Rachel Kalmann,[17] Saskia M. Imhoff,[17] Johan H. van Es,[1,2] Carmen López-Iglesias,[5] Peter J. Peters,[5] Bart L. Haagmans,[4] Wei Wu,[3] and Hans Clevers[1,2,18,20,*]

[1]Hubrecht Institute, Royal Netherlands Academy of Arts and Sciences (KNAW), University Medical Center, Utrecht, the Netherlands
[2]Oncode Institute, Hubrecht Institute, Utrecht, the Netherlands
[3]Singapore Immunology Network (SIgN), Agency for Science, Technology and Research (A*STAR), and Department of Pharmacy, National University of Singapore, Singapore, Singapore
[4]Viroscience Department, Erasmus University Medical Center, Rotterdam, the Netherlands
[5]Maastricht Multimodal Molecular Imaging Institute, Maastricht University, Maastricht, the Netherlands
[6]Department of Ocular Pathology and Imaging Science, Kyushu University, Fukuoka, Japan
[7]Singapore Eye Research Institute, Singapore, Singapore
[8]Ophthalmology and Visual Sciences Academic Clinical Program, Duke-NUS Medical School, Singapore, Singapore
[9]Department of Pediatrics, Yong Loo Lin School of Medicine, National University of Singapore, Singapore, Singapore
[10]National University Health System, Singapore, Singapore
[11]Immunology Program, Life Sciences Institute, National University of Singapore, Singapore, Singapore
[12]NUSMED Immunology Translational Research Program, National University of Singapore, Singapore, Singapore
[13]Singapore Institute for Clinical Sciences (SICS), Agency for Science, Technology and Research (A*STAR), Singapore, Singapore
[14]International Research Center for Medical Sciences, Kumamoto University, Kumamoto, Japan
[15]Department of Cell Biology-Inspired Tissue Engineering, MERLN Institute for Technology-Inspired Regenerative Medicine, Maastricht, the Netherlands
[16]University Eye Clinic Maastricht, Maastricht University Medical Center, Maastricht, the Netherlands
[17]Department of Ophthalmology, University Medical Center, Utrecht, the Netherlands
[18]Present address: Pharma, Research and Early Development of F. Hoffmann-La Roche Ltd., Basel, Switzerland
[19]These authors contributed equally
[20]Lead contact
*Correspondence: m.bannier@hubrecht.eu (M.B.-H.), h.clevers@hubrecht.eu (H.C.)
https://doi.org/10.1016/j.stem.2023.12.008

SUMMARY

The conjunctival epithelium covering the eye contains two main cell types: mucus-producing goblet cells and water-secreting keratinocytes, which present mucins on their apical surface. Here, we describe long-term expanding organoids and air-liquid interface representing mouse and human conjunctiva. A single-cell RNA expression atlas of primary and cultured human conjunctiva reveals that keratinocytes express multiple antimicrobial peptides and identifies conjunctival tuft cells. IL-4/-13 exposure increases goblet and tuft cell differentiation and drastically modifies the conjunctiva secretome. Human NGFR+ basal cells are identified as bipotent conjunctiva stem cells. Conjunctival cultures can be infected by herpes simplex virus 1 (HSV1), human adenovirus 8 (hAdV8), and SARS-CoV-2. HSV1 infection was reversed by acyclovir addition, whereas hAdV8 infection, which lacks an approved drug therapy, was inhibited by cidofovir. We document transcriptional programs induced by HSV1 and hAdV8. Finally, conjunctival organoids can be transplanted. Together, human conjunctiva organoid cultures enable the study of conjunctival (patho)-physiology.

INTRODUCTION

The conjunctiva lines the inner surface of the eyelid and covers the sclera (white of the eye). It consists of a stromal layer containing fibroblasts, blood vessels, and immune cells covered by a non-keratinizing stratified epithelium.[1] Two differentiated epithelium cell types have been discerned: mucus-producing goblet cells and water-secreting keratinocytes that expose mucins on their apical surface.[1] Most studies on the conjunctiva have focused on goblet cells since these—together with the tear gland—produce the mucin layer of the tear film that covers the ocular surface.[2] This mucin layer is essential for tear film homeostasis: it allows the aqueous layer of the tears to adhere to the ocular surface and protects against evaporative dry eye disease.[2] However, neither a role of conjunctival keratinocytes beyond creating

a mucin-rich epithelial barrier nor the identity of the conjunctival stem cell have been uncovered.[3]

Studies on the ocular surface have primarily focused on one tissue essential for vision, the cornea.[4] Nevertheless, the conjunctiva is similarly essential for sight: its malfunction eventually affects corneal homeostasis and can lead to blindness. It is the conjunctiva that provides immune protection to the ocular surface.[5] Second, if physical or viral insults damage the conjunctiva, the tear film is destabilized,[6] leading to dry eye disease, discomfort, and eventually blindness.[7] A major hurdle to the understanding of conjunctival homeostasis and disorders is the lack of a representative *in vitro* model. Indeed, models of the conjunctival epithelium established over the years hold several limitations: they are either short-lived explants cultured under poorly defined conditions (i.e., on feeder cells or amniotic membranes) or are derived from induced pluripotent stem cells that typically do not recapitulate the cellular diversity and maturity of the conjunctival epithelium.[8–16] However, no protocol is available that allows the growth of primary conjunctival tissue long-term and under defined conditions.

Long-term expanding, adult stem cell-based organoids were first established from intestinal tissue.[17] Organoids are three-dimensional structures that recapitulate essential architecture and functions of the tissue of origin. Organoids can model aspects of human physiology and disease in controlled environments.[18] Here, we establish mouse and human organoids derived from primary conjunctiva, show that they recapitulate key features of the conjunctival epithelium, and provide a versatile platform to study conjunctival (patho-)physiology.

RESULTS

Establishment of mouse conjunctiva organoids

We optimized existing protocols to establish conjunctiva organoids from primary mouse tissue. Wild-type conjunctiva from eyelids and sclera was dissected and trypsinized before plating in basement membrane extract (BME). The culture medium contained B27, N-acetylcysteine, EGF, FGF1, Noggin, R-spondin 1, transforming growth factor β (TGF-β) inhibitor, and Rho-kinase inhibitor. B27, EGF, and Rho-kinase inhibitor appeared essential for organoid outgrowth (Figures 1A and S1A). After 3–4 days, dense organoids appeared (Figure 1B). Organoids were split every 7 days and could be maintained for at least 36 passages (Figures 1B and S1B). All media components, except for EGF, were essential to sustain organoid long-term growth (Figure S1C). Expression of conjunctival markers was stable over passaging (Figure S1D). Organoids expressed the conjunctival marker KRT19 and the master transcription factor of eye development PAX6 (Figure 1C). TP63+ cells were located basally and MUC1+ keratinocytes apically in both mouse tissue and organoids (Figure 1C). Of note, the outside surface of adult stem cell-derived organoids contacts the BME and invariably represents the basal side of the corresponding epithelium.[18] These expanding mouse conjunctival organoids did not contain MUC5AC+ goblet cells (Figure 1C).

PAX6 is essential for conjunctival differentiation

PAX6 is the master regulator of eye development and maintains expression in the conjunctiva during adulthood. PAX6 expression is reduced in certain conjunctival pathologies, such as pterygium and pinguecula.[19,20] To assess the effect of PAX6 loss of function in conjunctival organoids, we mutated *Pax6* with CRISPR-Cas9 (*Pax6* knockout [$Pax6^{KO}$], Figures 1D–1F and S1E). Using bulk RNA sequencing, we found 709 downregulated genes and 454 upregulated genes in $Pax6^{KO}$ compared with $Pax6^{WT}$ organoids (Figure 1G; Table S1). Among the genes that were downregulated in $Pax6^{KO}$ organoids, we found several that encode secreted proteins, such as the antimicrobial peptides *Ltf*, *Slpi*, *Pigr*, and *Lcn2*, the surfactant protein *Sftpd* and *Fcgbp* involved in maintaining gel structures, as well as the complement factors *C3* and *Cfh*. We also noted that Toll-like receptors 2 and 4 (*Tlr2* and *Tlr4*) were downregulated (Figure 1G). Conversely, genes that were upregulated in $Pax6^{KO}$ organoids included stem cell-related genes, such as the Wnt target *Axin2* and the basal cell markers *Trp63*, *Trp73*, *Krt5*, and *Krt14* (Figure 1G).[21,22] Immunohistochemistry confirmed that $Pax6^{KO}$ organoids showed increased expression of TP63 and decreased levels of PAS mucus staining (Figure 1H). Pterygia similarly harbored increased *TP63* expression and loss of differentiation markers (including *MUC1*, *MUC5AC*, and *LCN2*) (Figure S1F).[23] In conclusion, PAX6 loss resulted in an undifferentiated basal-like phenotype, similar to that seen in pterygia.[19,20,23]

Establishment of human conjunctiva organoids

We then set out to establish human-derived conjunctiva organoids. We obtained conjunctival biopsies from deceased donors and patients undergoing ocular surgeries. Biopsies were sampled from palpebral (eyelid) and bulbar (eyeball) conjunctiva and trypsinized. Single cells were then plated in BME in the mouse conjunctival medium supplemented with WNT surrogate, FGF10, and the cyclic AMP activator forskolin (FSK). Besides, EGF was removed as it reduced the lifespan of the organoids (Figures 2A, S1G, and S1H). We obtained dense organoids from both bulbar and palpebral conjunctiva that were split every 9–14 days for up to 12 passages for bulbar lines and 17 passages for palpebral lines (Figures 2B and S1G). Withdrawal of individual medium components did not impact the original organoid outgrowth but impaired long-term passaging (except for N-acetylcysteine) (Figure S1H). Organoids retained expression of the conjunctival marker KRT19 and contained TP63+ basal cells, similar to the original tissue (Figures 2C and S1I). Although organoids did not contain MUC5AC+ goblet cells under these expansion conditions, they contained differentiated PAS+, MUC1+, and AQP5+ keratinocytes, morphologically very similar to tissue keratinocytes (Figures 2C and S1I). Of note, AQP5 expression is in line with the ability of conjunctival keratinocytes to secrete water.[24]

Differentiation of human conjunctiva organoids

To differentiate human conjunctiva organoids toward goblet cell fate, we removed WNT surrogate, FGF1, FGF10, and B27 from the medium (Figure 2D). Upon exposure for 9 days to the differentiation medium, organoids became cystic and displayed increased expression of the goblet cell transcription factor *SPDEF* and the secreted mucin gene *MUC5AC* (Figures S1J and S1K).[25,26] Exposure to differentiation medium for 7 days reduced the number of TP63+ basal cells while increasing the numbers of MUC5AC+ cells (Figure 2E). KRT19 remained expressed by all cells in differentiation medium, and MUC1

CellPress
OPEN ACCESS

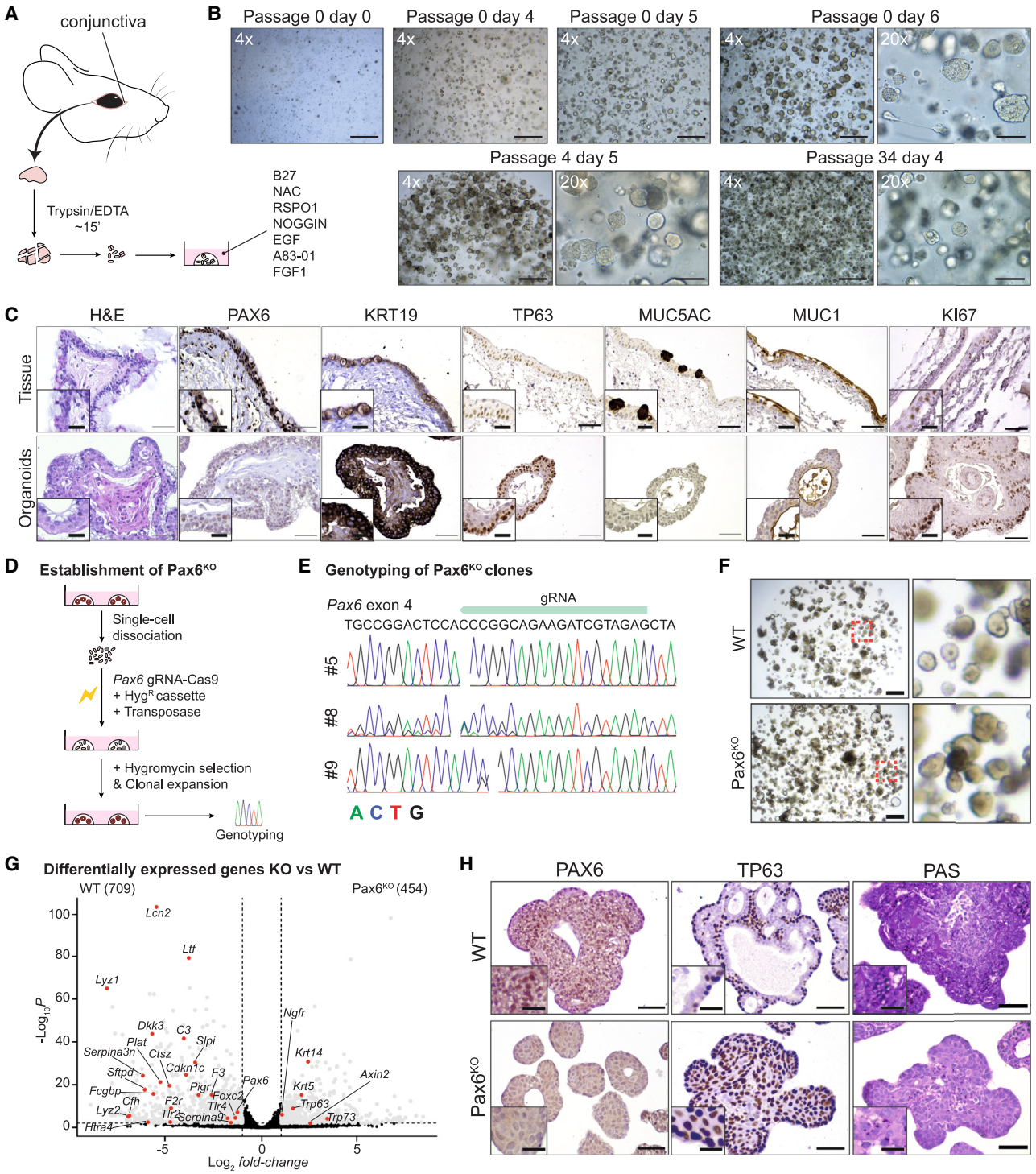

Figure 1. Mouse conjunctival organoids require PAX6 to differentiate

(A) Workflow.

(B) Organoid outgrowth and morphology after up to 34 passages. Scale bars, 500 μm (4× pictures) and 100 μm (20× pictures).

(C) Staining for the indicated markers in mouse conjunctiva organoids compared with mouse conjunctival tissue. Scale bars, 50 μm. Insets scale bars, 20 μm.

(D) Schematic of the establishment of *Pax6* knockout (Pax6^{KO}).

(E) Sequencing traces of Pax6^{KO} clones.

(F) Bright-field images of representative WT and Pax6^{KO} clones at, respectively, passage 32 and 25, 13 days after split. Scale bars, 500 μm.

(G) Differentially expressed genes between WT (n = 2 lines) and Pax6^{KO} (n = 3 lines) organoids. Light gray: fold-change (fc) > 2 and p-adjusted < 0.01.

(H) Staining for PAX6, TP63, and PAS in WT and Pax6^{KO} clone 5. Scale bars, 50 μm; insets, 20 μm. Related to Figure S1 and Table S1.

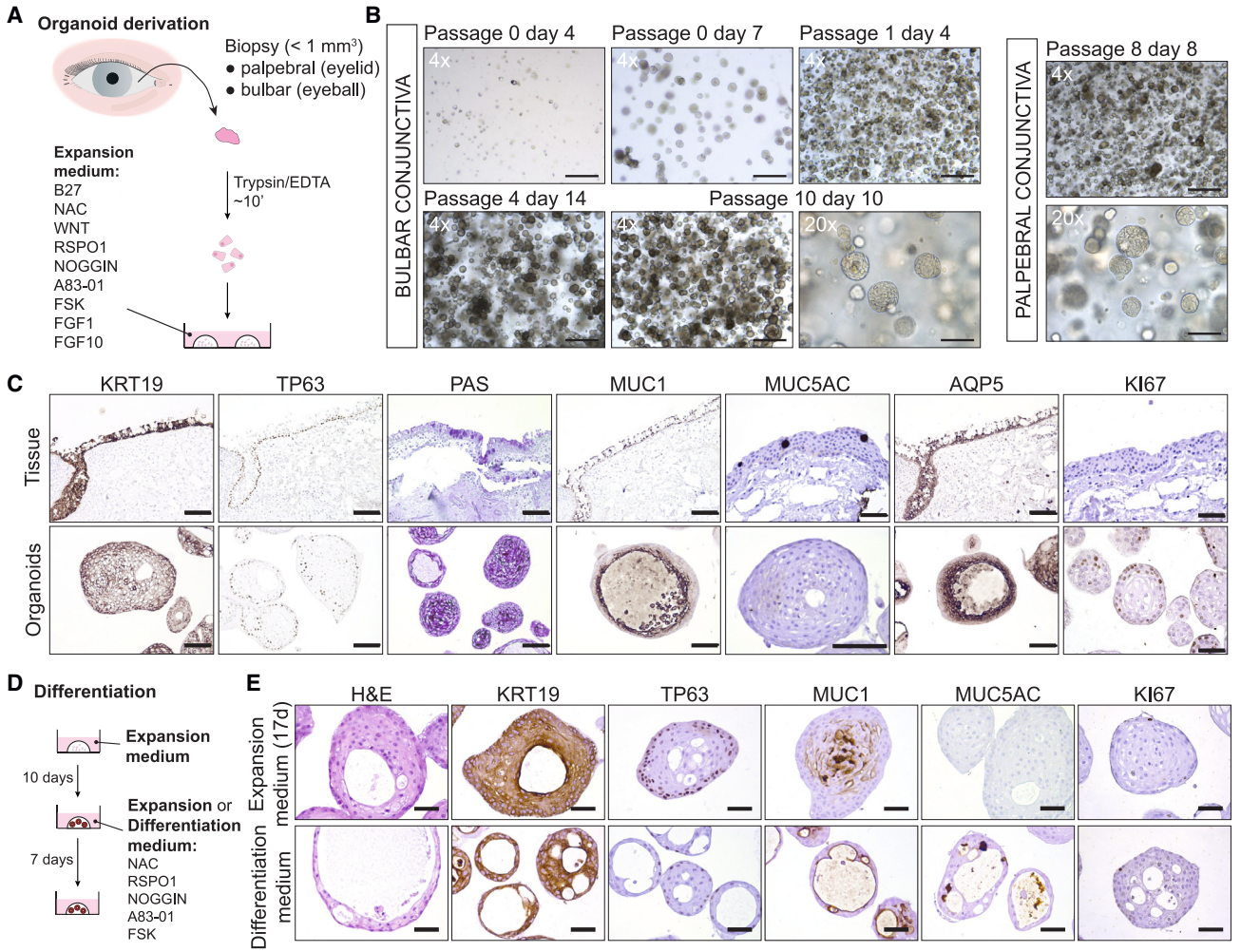

Figure 2. Establishment, characterization, and differentiation of human conjunctiva organoids

(A) Schematic of human conjunctival organoid establishment.

(B) Bright-field images of organoid outgrowth and organoid morphology. Scale bars, 500 μm (4× pictures) and 100 μm (20× pictures).

(C) Staining for the indicated markers in human conjunctiva organoids and tissue. Scale bars, 50 μm.

(D) Schematic of human conjunctival organoid differentiation.

(E) Staining for the indicated markers of human conjunctiva organoids cultured in expansion and differentiation media after 17 days in culture. Scale bars, 50 μm. Related to Figure S1.

remained apical (Figure 2E). Of note, MUC5AC staining was also detected in the lumen of some organoids, suggesting this mucin could be secreted (Figure 2E).

ALI culture of human conjunctiva organoids promotes goblet cell differentiation

Air-liquid interface (ALI) cultures of epithelia that are normally exposed to air can promote near-native differentiation of cultured cells, such as has been shown for the upper airway.[27] Thus, we seeded conjunctival organoid cells on collagen-coated transwells in human expansion medium. When cells reached confluency—which usually occurred within 3–4 days—we removed the liquid in the upper chamber to create an ALI (Figure 3A). We followed the ALI cultures for up to 22 days, during which they remained confluent. At day 4 after shifting to ALI, the cultures were 2–3 cell layers thick and displayed basal TP63+ cells and apical MUC1+ keratinocytes, but no MUC5AC+ goblet cells (Figure 3B). After 17 days, the cultures had become 5–10 cell layers thick (Figure 3B). Small and densely packed TP63+ cells constituted the 2–3 basal-most layers (Figure 3B). The number of proliferative cells decreased over time to reach similar numbers as seen in primary tissue at 17 days post-ALI (Figures 2C and S1L). No substantial apoptosis was detected (Figure S1M). MUC1 was expressed in all cells, with a gradual increase toward the apical surface (Figure 3B).

Notably, 17-day-old ALI cultures contained MUC5AC+ cells (Figures 3B and 3C). These MUC5AC+ cells resembled tissue goblet cells, with enlarged PAS+ vacuoles and containing MUC5AC+ vesicles (Figures 3B, 3C, and S1N). In addition, the ultrastructure of these cells was comparable to that of tissue goblet cells (Figure 3D).[28] Besides, differentiated ALI cultures expressed higher levels of *SPDEF* and *MUC5AC* in comparison

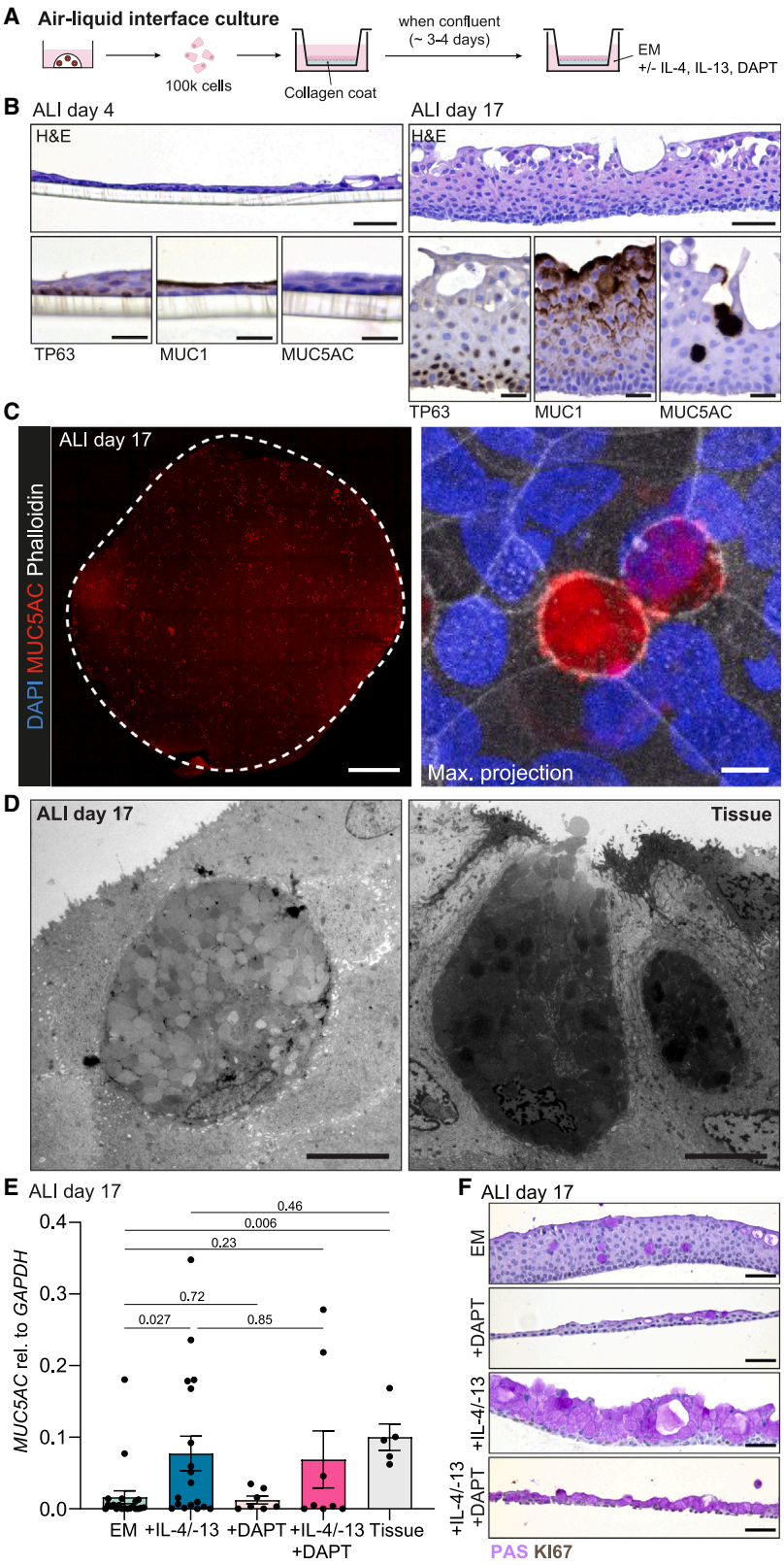

Figure 3. Goblet cell differentiation is enhanced by ALI culture and exposure to IL-4 and IL-13

(A) Workflow.

(B) Staining for the indicated markers of human conjunctiva ALI cultures 4 and 17 days after shifting to ALI. Scale bars, 50 μm.

(C) Staining for MUC5AC (red), phalloidin (white), and DAPI (blue) in an entire transwell (top, scale bars, 1 mm). An inset is shown below (scale bars, 10 μm).

(D) Transmission electron microscopy of a goblet cell in a 17-day-old ALI culture (left) and in primary tissue (right). Scale bars, 5 μm. See also Figure S1.

(E) Expression of MUC5AC in 17-day-old ALI cultured with EM only, or supplemented with IL-4/-13, with DAPT, or with both as assessed by qPCR. A tissue control is shown. Each dot represents an independent experiment from at least 3 different donors per condition. Error bars: standard error to the mean (SEM).

(F) PAS and KI67 staining in ALI exposed to EM only or EM supplemented with IL-4/-13, DAPT, or both. Scale bars, 50 μm. Related to Figure S1.

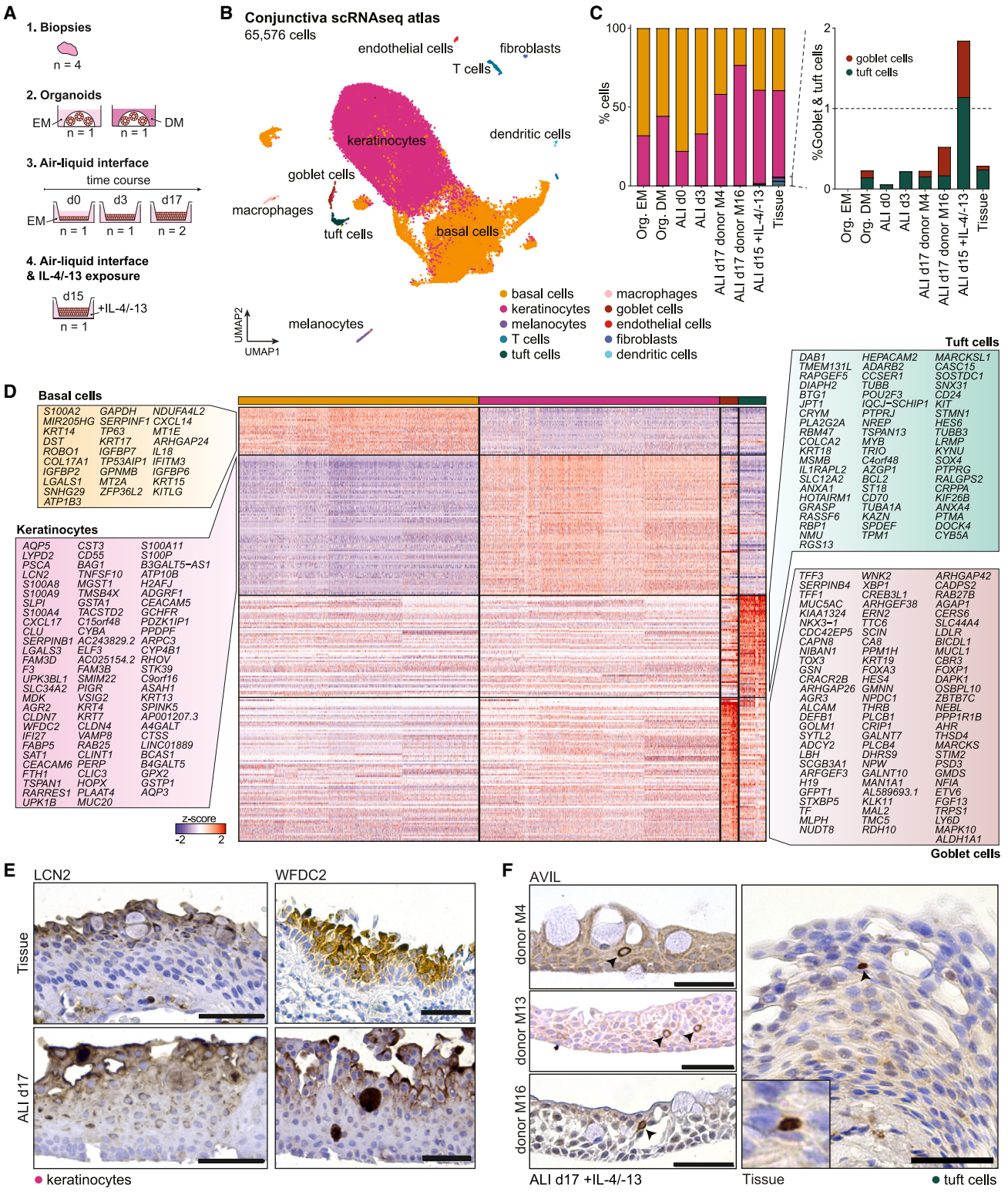

Figure 4. Single-cell mapping of the conjunctiva reveals the gene expression signature of keratinocytes and the presence of tuft cells

(A) Samples subjected to single-cell RNA sequencing.

(B) Uniform manifold approximation and projection (UMAP) cell embedding of the conjunctival cells colored by cell type.

(C) Contribution of cell types to each sample.

(legend continued on next page)

with their 3D organoid counterparts, be it in expansion or in differentiation medium (Figure S1K). Together, conjunctiva organoid-derived ALI cultures recapitulated the architecture and cell-type composition of human conjunctival tissue.

Interleukin signaling enhances goblet cell differentiation

Interleukins, including interleukin (IL)-4 and IL-13, have previously been implicated in conjunctival goblet cell expansion.[29–31] Hence, IL-4 and IL-13 were added to the expansion medium in the bottom chamber when shifting the cultures to ALI. After 17 days, goblet cell differentiation had increased compared with expansion medium-exposed ALI cultures (Figures 3E and 3F). NOTCH has also been described to be required for conjunctival goblet cell differentiation.[32] In ALI cultures, NOTCH inhibition did not affect goblet cell differentiation—even when induced by IL-4/-13—but rather reduced conjunctival stratification (Figures 3E and 3F).

Single-cell characterization of human conjunctival tissue and cultures

To compare our newly established culture systems directly to conjunctival tissue, we applied single-cell mRNA sequencing to (1) tissue biopsies, (2) organoids cultured in expansion or differentiation medium, (3) ALI cultures 0, 3, and 17 days after shifting to ALI, and (4) ALI cultures exposed to IL-4/-13 for 15 days (Figure 4A). Following quality controls, a total of 65,576 cells remained (Figures 4B, 4C, and S2A–S2C). Based on the expression of established markers, we first identified stromal cell types uniquely present in the tissue biopsies (melanocytes, T cells, macrophages, dendritic cells, endothelial cells, and fibroblasts) and four epithelial cell types present both *in vivo* and *in vitro* (Figures 4B and S2D; Table S2).

Conjunctival basal cell populations

The 26,295 basal cells marked by *TP63, COL17A1*, and *KRT15* were heterogeneous (Figures 4B, 4D, S2D, S3A, and S3B; Tables S2 and S3). Firstly, we identified 3 clusters of cycling basal cells, respectively marked by *PTTG1*, *PCLAF*, and *HELLS* (Figures S3A–S3D). These cycling cells were most present in early ALI cultures (~22% of all cells), organoids (~17% in expansion, ~8% in differentiation), and ALI cultures treated with interleukins (~6%), rather than in biopsies (~2.5%) and in ALI day 17 (~3%) (Figures 4C and S3C). Interestingly, similar basal cell populations were previously described in the skin interfollicular epidermis.[33] We found 5 populations of non-cycling basal cells that expressed high levels of *LGR4*, *SERPINF1*, *DPP6*, *PLAU*, and *KRT17*, respectively (Figures S3A–S3D). Lastly, four distinct populations (marked by *SERPINB1, PTPRJ*, *CXCL17*, or *KRT23*) exhibited characteristics of early keratinocytes and expressed differentiation markers such as *LCN2*, *AQP5*, and *MUC16* (Figures S3A–S3D). Of note, *DPP6*+ basal cells and *KRT23*+ early keratinocytes were only present in culture, whereas *CXCL17*+ cells almost exclusively originated from a single tissue donor (Figure S3C).

NGFR+ cells are conjunctival bipotent stem cells

NGFR, a stem cell marker in multiple organs,[34] was enriched in conjunctival basal cells (Figure S3E). We probed the organoid-forming capacity of sorted *NGFR*+ and *NGFR*− cells (Figures S3F–S3H). Only NGFR+ cells were able to generate organoids (Figure S3H). One question in the field is whether conjunctival stem cells can generate both goblet cells and keratinocytes.[3] We identified both MUC1+ keratinocytes and MUC5AC+ goblet cells in organoids derived from single NGFR+ cells (Figure S3I). In sum, this experiment provided definitive evidence for NGFR+ cells as bipotent conjunctiva stem cells.

Molecular signature of conjunctival keratinocytes

The function of keratinocytes has not been detailed to date. Beyond the typical keratinocyte markers (*MUC1* and *MUC20*), we found that keratinocytes expressed genes involved in secretion, defense response, and immune cell activation (Figure 4D). Among these genes, keratinocytes expressed antimicrobial proteins *PIGR*, *WFDC2*, *S100A4*, *S100A8*, *S100A9*, *SLPI*, and *LCN2* (Figure 4D; Table S2). Similarly to other mucosal tissues, keratinocytes expressed the *CXCL17* chemokine, key to recruit antigen-presenting cells[35] (Figure 4D; Table S2). We confirmed by antibody staining that keratinocytes in ALI cultures expressed LCN2 and WFDC2, similar to tissue samples (Figure 4E). Together, this implied a central role of conjunctival keratinocytes in protecting the ocular surface.

Conjunctival tuft cells

Tuft cells are a rare cell type found in several epithelia and involved in immune responses.[36] Tuft-like cells were identified in the mouse conjunctival epithelium previously[37] but, to our knowledge, were never reported in human conjunctiva. We identify a rare population of tuft cells present both in tissue and culture with a distinct gene expression signature (Figures 4B–4D and S4A–S4C; Table S2). Conjunctival tuft cells expressed genes involved in synapse organization (Figure S4B). More specifically, these expressed several established tuft cell markers such as *HOTAIRM1*, *TUBA1A*, and the transcription factors *SOX4* and *POU2F3* (Figures 4D and S4A–S4C; Table S2).[36,38,39] As tuft cell heterogeneity was previously described,[36] we subclustered the conjunctival tuft cells (Figures S4D and S4E). This defined three conjunctival tuft cell states, all expressing *SOX4* and *POU2F3* (Figures S4D–S4F; Table S3). *KRT13*+ tuft cells expressed stem cell markers (*KRT13*, *KRT5*, and *TP63*) and gene ontology (GO) terms involved in epidermis development and keratinocyte differentiation (Figures S4G–S4I; Table S3). *NREP*+ tuft cells expressed the neuronal markers *NREP*, *TUBB3*, and *NMU* and overall had an axonogenesis gene expression program (Figures S4G, S4J, and S4K; Table S3). *BMX*+ tuft cells expressed mature tuft cell markers *AVIL* and *BMX* (Figures S4G and S4L; Table S3). This suggests that these three conjunctival tuft cell populations could perform different functions *in vivo*. Lastly, we confirmed

(D) Top differentially expressed genes between basal cells, keratinocytes, goblet cells, and tuft cells ($p < 0.01$).
(E) Staining for markers enriched in keratinocytes LCN2 and WFDC2 in tissue and 17-day-old ALI cultures.
(F) Staining for the tuft cell marker AVIL in 17-day-old ALI bulbar (donors 4 and 13) and palpebral (donor M16) cultures exposed to IL-4/-13 for 17 days and in bulbar tissue. Scale bars, 50 μm. Related to Figures S2–S6 and Tables S2, S3, S4, and S5.

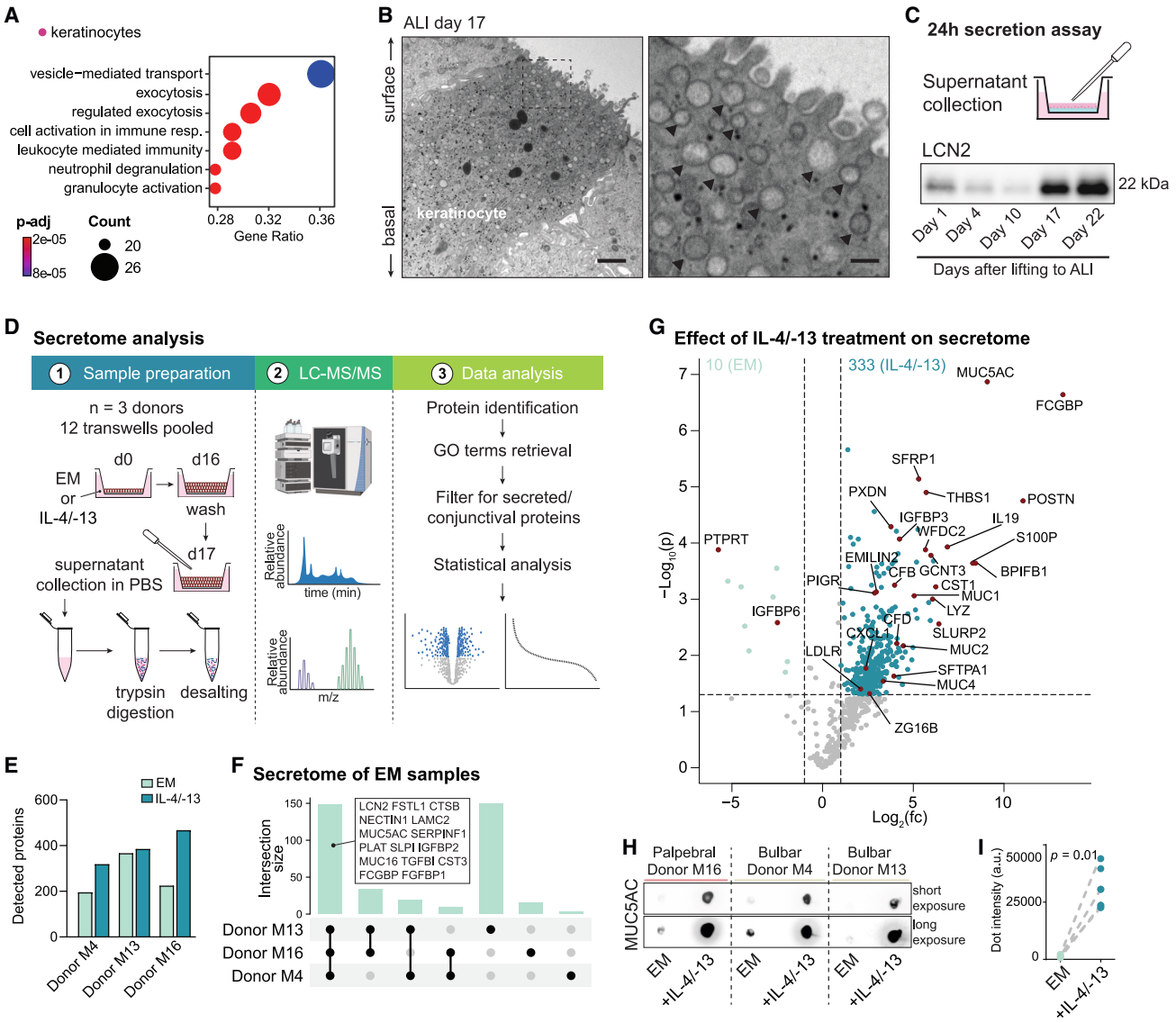

Figure 5. Analysis of the conjunctival secretome

(A) GO terms enriched in the keratinocyte gene signature (from Figure 4).

(B) Electron microscopy image of a keratinocyte in a 17-day-old ALI culture. Arrowheads point at vesicles present at the apical surface of the ALI culture. Left scale bars, 1 μm; right, 200 nm.

(C) LCN2 secretion assay was performed on ALI cultures 1, 4, 10, 17, and 22 days after beginning ALI.

(D) Workflow.

(E) Number of detected proteins per sample. n = 3 donors.

(F) Upset plot of the detected proteins in ALI cultures cultured with EM only (baseline secretion).

(G) Differentially secreted proteins upon IL-4/-13 exposure. Blue: $p < 0.05$ and $fc > 2$.

(H) Dot blot for MUC5AC in the supernatant of 17-day-old ALI exposed to IL-4/-13 or not from three donors. Top: short exposure, bottom: long exposure.

(I) Quantification of dot intensity. Related to Figure S6 and Table S5.

histologically the presence of AVIL+ tuft cells in primary conjunctiva tissue and ALI cultures (Figure 4F).

Transcriptome of conjunctival goblet cells

Conjunctival goblet cells have been the main focus of conjunctival research in the past years but were never transcriptionally characterized. The dataset contained goblet cells from tissue biopsies and cultures treated with or without IL-4/-13 (Figure 4B). As expected, the representation of goblet cells in the IL-4/-13-treated ALI cultures was increased (Figure 4C). All goblet cells expressed a glycosylation gene program, including *SPDEF* and *MUC5AC*, which was the most prominent difference with keratinocytes (Figures 4D and S5A–S5E; Tables S2 and S5). Subclustering of the goblet cells identified 2 subpopulations: *S100A8*+ and *TFF3*+ goblet cells (Figures S5C–S5J; Table S4). Beyond the secreted mucous stabilizers *TFF1* and

TFF3, *TFF3*+ goblet cells expressed higher levels of *MUC5AC* and a large repertoire of genes involved in ion transport (*WNK2* and *STK39*), regulation of GTPase activity (*ARFGEF3* and *TRIO*), and JNK signaling (*MAPK10* and *MAP4K4*) (Figures S5G and S5H; Table S4). *S100A8*+ goblet cells expressed genes promoting neutrophil activation (*PIGR*, *B2M*, and *S100A8*) and regulating peptidase activity (*SLPI* and *CST3*) (Figures S5F, S5I, and S5J; Table S4). These two distinct goblet cell populations are likely to perform different functions *in vivo*. Transcriptionally, conjunctival goblet cells were most similar to stomach goblet cells, partly because both expressed *MUC5AC* (Figures S5K and S5L; Table S4). The expression of *S100A8*, *LY6D*, and *LYPD2*, however, was specific to conjunctival goblet cells (Figure S5L; Table S4).

Effect of IL-4/-13 on the transcriptional profile of the conjunctival epithelium

Interleukins 4 and 13 are cytokines involved in type II inflammatory response.[40] *In vitro*, IL-4/-13 exposure increased numbers of goblet and tuft cells (Figures 3E, 3F, 4C, and S6A). We found 22 significantly differentially expressed genes upon IL-4/-13 exposure across all epithelial cell types (Figures S6B–S6E; Table S5). Both basal cells and keratinocytes treated with IL-4/-13 expressed higher levels of *POSTN*, an extracellular matrix (ECM) protein involved in wound repair upregulated in allergic conjunctivitis (Figures S6B and S6C).[41] Keratinocytes additionally displayed increased expression of the complement factor *CFD* and lower levels of *AQP5* (Figure S6C). The only gene affected by IL-4/-13 treatment in tuft cells was the phospholipase *PLA2G2A* (Figure S6D). In goblet cells treated with IL-4/-13, the bicarbonate transporter *SLC4A4*, essential for mucus secretion and clearance in the airway, was upregulated, whereas *TFF3* was downregulated (Figure S6E).[42,43] By staining, we indeed found TFF3-negative and SLC4A4-positive goblet cells in ALI exposed to IL-4/-13 (Figures S6F and S6G). Hence, the conjunctival epithelium underwent limited transcriptional remodeling after 15 days of IL-4/-13 exposure.

Functionality of conjunctival epithelium *in vitro*

It is established that conjunctival goblet cells secrete most of the mucus layer covering the ocular surface.[2] We found that keratinocytes expressed antimicrobial peptides and genes involved in exocytosis (Figures 4D, 4E, and 5A). Medium-size secretory vesicles were present in some, but not all, conjunctival keratinocytes of ALI cultures (Figure 5B). More specifically, LCN2—a marker enriched in keratinocytes—was secreted in the supernatant in increasing quantities as the ALI cultures aged and differentiated (Figure 5C). Hence, the conjunctival epithelium derived from organoids secreted antimicrobial peptides.

Mapping the conjunctival secretome

To map the conjunctival secretome, we established ALI cultures from 3 individual donors treated or not with IL-4/-13 for 17 days (Figure 5D). The supernatant produced was analyzed by liquid chromatography-tandem mass spectrometry (LC-MS/MS) (Figure 5D). Across all samples, we detected 640 quantifiable unique proteins, with, on average, more proteins detected in supernatants from IL-4/-13-exposed ALI cultures (Figures 5E and S6H; Table S5). Importantly, supernatants were enriched for secreted proteins (Figure S6I). In the baseline conjunctival secretome (without interleukins), 148 proteins were detected in all samples, which participated to neutrophil activation and with antimicrobial peptidase activity (Figures 5F and S6J). Upon IL-4/-13 exposure, the secretion of 333 proteins was upregulated (Figure 5G). These proteins were implied in hemostasis (THBS1 and IL-19), ECM remodeling (POSTN), peptidase activity (LYZ), innate immune response activation (PIGR, CFD, and CFB), and glycosylation (MUC5AC, MUC1, and MUC4) (Figures 5G and S6K). We confirmed by antibody staining that MUC5AC was enriched in the supernatants of IL-4/-13-treated ALI (Figures 5H and 5I). Of note, most proteins upregulated upon IL-4/-13 exposure were not differentially regulated at the single-cell transcriptional level (Figure S6L). This suggests that the shift in conjunctival secretome composition results from a shift in the balance of the different cell types, a translational regulation, and/or a secretion regulation. Overall, the conjunctival epithelium responds to inflammatory signals *in vitro*.

SARS-CoV-2 infects the conjunctiva *in vitro*

One major cause of inflammation is viral conjunctivitis, which can be caused a.o. by herpes simplex virus 1 (HSV1), human adenovirus 8 (hAdV8), and severe acute respiratory syndrome coronavirus 2 (SARS-CoV-2). Although HSV1 represents 5% of all conjunctivitis. Adenoviruses account for 90% of all conjunctivitis, of which hAdV8 is the most common strain worldwide.[44] Besides, ~1% of patients with SARS-CoV-2 present with conjunctivitis.[45] These viruses can infect the conjunctiva and the cornea, resulting in a sight-threatening condition.[46–48] Viral conjunctivitis has been hard to study in the lab due to a lack of long-term *in vitro* models. As our newly established conjunctival cultures expressed the identified/potential viral entry receptors for each of these viruses (Figure S7A),[49–51] we used ALI cultures to model viral conjunctivitis. To investigate whether these viruses can infect the conjunctiva, we applied each of these apically to differentiated ALI cultures for 3 h and incubated for up to 4 days with or without candidate inhibitors (Figure 6A). Both variants of SARS-CoV-2 replicated in the conjunctiva *in vitro* (Figures 6B and 6C). Furthermore, the produced virus collected in ALI supernatant possessed secondary infection potential (Figure S7B).

HSV1 infection

For modeling HSV1 infection, we used a strain whose capsid protein VP26 was tagged with tdTomato (hereafter called HSV1-tdTomato).[52] HSV1 titer increased by 5 logs over a course of 96 h after initial incubation with HSV1, implying a productive infection of the conjunctival ALI (Figures 6D, 6E, and S7C). Interestingly, we noted tdTomato+ foci in cells, presumably the virus assembly sites in the nuclear envelope (Figure S7D).[52] tdTomato+ cells also displayed cytopathic effects (CPEs), including cell rounding and exclusion from the epithelial layer, resulting in large gaps in the ALI culture (Figures S7D and S7E). HSV1 infection was blocked by acyclovir, an inhibitor of HSV1 DNA polymerase, commonly given to patients with HSV1-induced conjunctivitis (Figures 6D and 6E).[53] To gain insight into the conjunctival epithelium's response to HSV1, we performed bulk RNA sequencing of infected ALI and their uninfected counterparts (Figures 6F and S7F–S7H; Table S6). As expected, HSV1-infected samples increased expression of genes involved

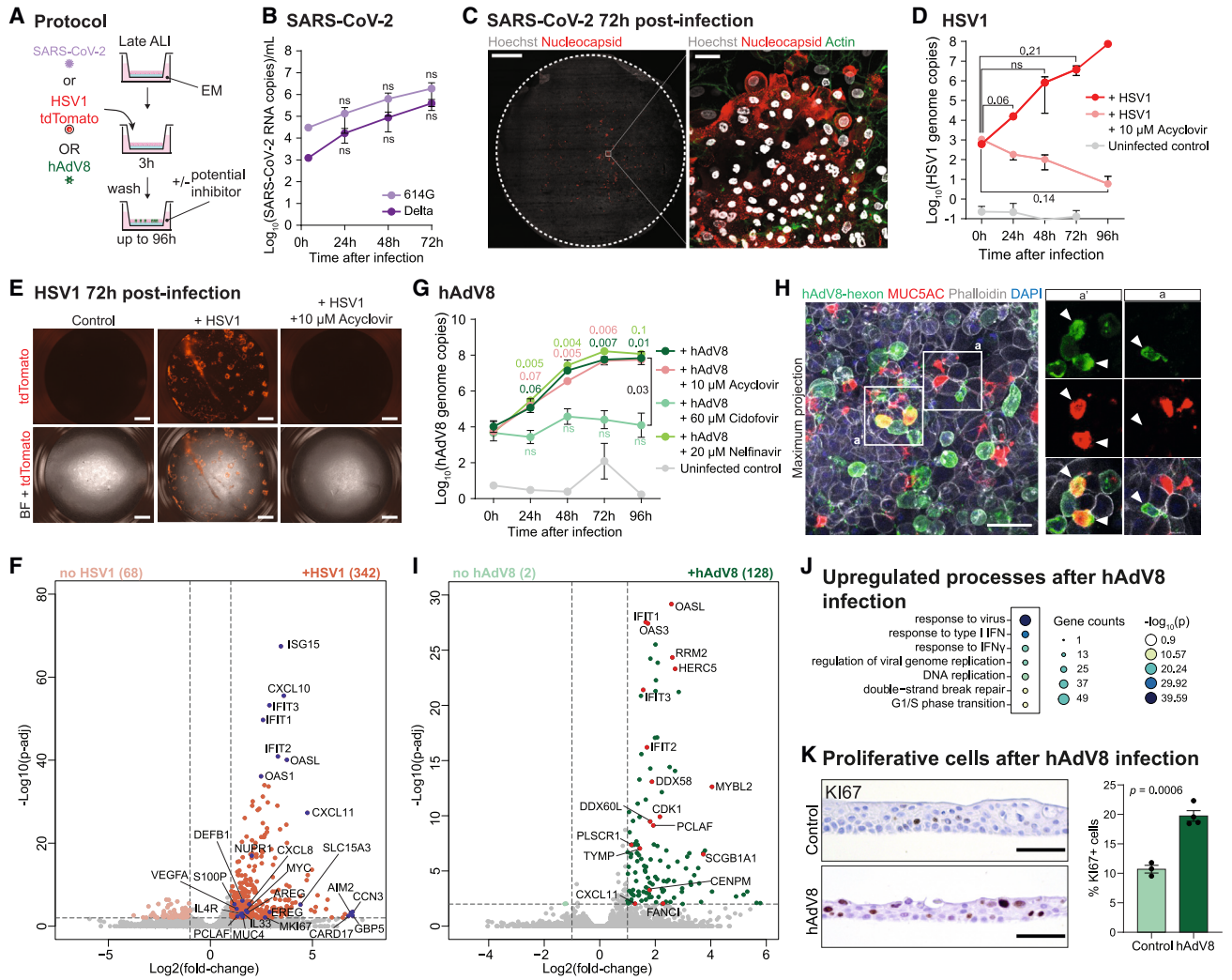

Figure 6. Conjunctival air-liquid interfaces sustain SARS-CoV-2, HSV1, and hAdV8 infection

(A) Infection protocol.

(B) SARS-CoV-2 variants 614G and Delta titers in conjunctival ALI cultures detected by qPCR. n = 3 independent infected ALI cultures.

(C) Staining for stained for SARS-CoV-2 variant Delta nucleocapsid (red), actin (green), and Hoechst (white) in infected ALI culture. Scale bars, 1 mm (left) and 30 μm (right).

(D) HSV1 titers in conjunctival ALI cultures detected by qPCR, with and without 10 μM acyclovir treatment. n = 3 independent experiments.

(E) tdTomato signal in ALI cultures 72 h post-infection in uninfected (control) and HSV1 infected ALI cultures treated or not with 10 μM acyclovir. Top, tdTomato signal; bottom, overlap with bright field. Scale bars, 1 mm.

(F) Differentially expressed genes upon HSV1 infection (fc > 2; padj < 0.01).

(G) hAdV8 titers in conjunctival ALI cultures detected by qPCR, with and without 10 μM acyclovir, 60 μM cidofovir, or 20 μM nelfinavir treatment. n = 3 independent experiments. The color of the p value indicates to which condition it refers to.

(H) Infected ALI culture stained for hAdV8-hexon (green), MUC5AC (red), phalloidin (white), and DAPI (blue). Top panel is a maximum projection, whereas bottom insets are single z-planes. Arrowheads point at hAdV8 positive cells. Scale bars, 50 μm.

(I) Differentially expressed genes upon hAdV8 infection (fc > 2; padj < 0.01).

(J) Selected upregulated GO terms upon hAdV8 infection.

(K) KI67 staining in control and hAdV8-infected ALI cultures and quantification of KI67+ cells per ALI (n = 3 or 4 sections quantified per condition). Scale bars, 50 μm. All scale bars represent SEM. Related to Figure S7 and Table S6.

in viral response, including interferon-response genes (*ISG15*, *IFIT1*, and *IFIT2*), cytokines (*CXCL11*, *CXCL8*, and *IL33*), and antimicrobial proteins (*DEFB1* and *S100P*) (Figures 6F and S7G; Table S6). Interestingly, genes involved in positive regulation of angiogenesis were upregulated (including *VEGFA*), which is in line with symptoms of viral conjunctivitis (Figure S7H). Thus, organoid-derived ALI cultures support HSV1 infection and represent a human ocular surface model for HSV1 infection.

hAdV8 infection

Adenoviruses are the leading cause of viral conjunctivitis.[44] Yet, to date, no medication has been approved, partly because there

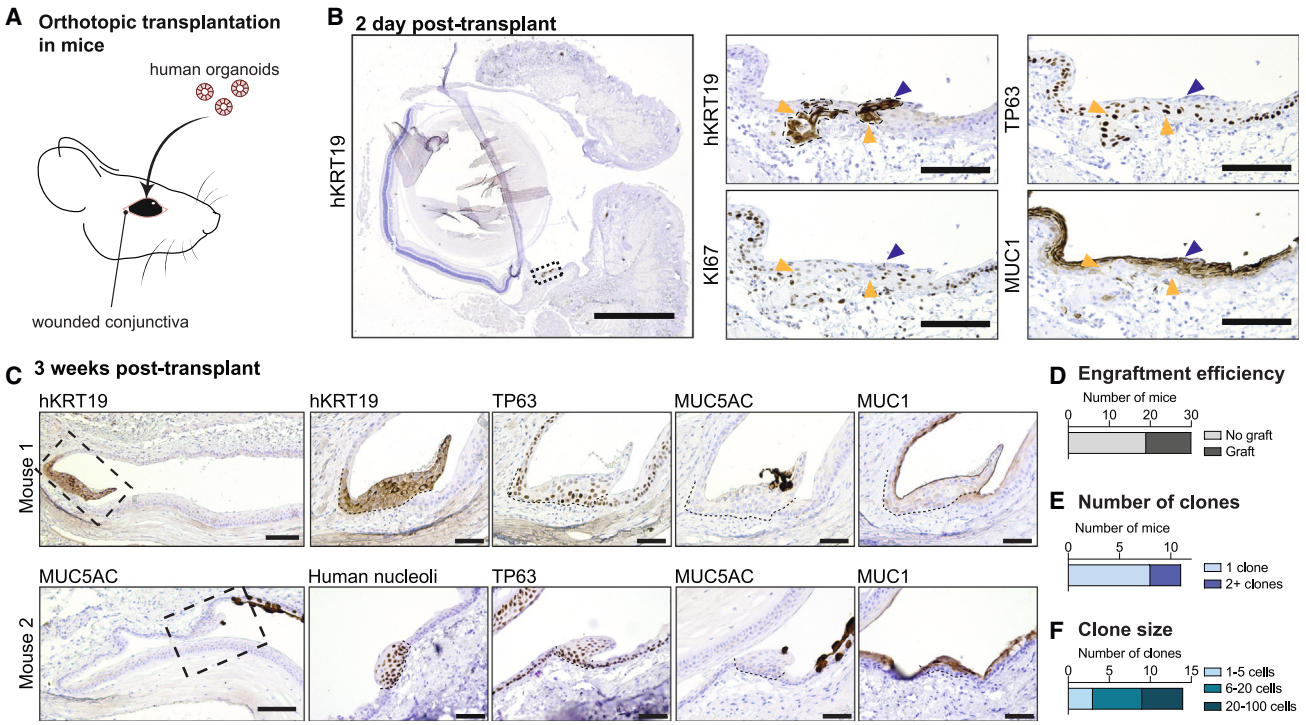

Figure 7. Human conjunctival organoids can engraft and be engineered for human transplantation

(A) Schematic of organoid transplantation in NSG mice.

(B) Staining for human KRT19 (hKRT19), KI67, TP63, and MUC1 in a transplanted eye 2 days after the surgery. Scale bars: large panel 500 μm and small panels 50 μm. Representative of n = 2 mice.

(C) Staining for hKRT19, human nucleoli, MUC5AC, MUC1, and TP63 3 weeks after transplantation. Dashed lines underline the graft location based on human stainings on immediately consecutive sections. Scale bars, left panels 100 μm and right panels 50 μm.

(D) Quantification of successful engraftment after 3 weeks (n = 30 mice).

(E) Number of clones (i.e., independent sites of engraftment) per engrafted eye 3 weeks post-transplant (n = 11 eyes).

(F) Clone size based on the human nucleoli staining 3 weeks post-transplant.

is no model system for this type of ocular infection. An hAdV8 strain, isolated from a patient,[54] was added to 17-day-old conjunctival ALI cultures (Figure 6A). Conjunctival ALI cultures were readily infected by hAdV8, as confirmed by the viral titer measured by qPCR (Figure 6G). CPEs were visible starting from 48 h after infection: infected cells darkened and were extruded from the epithelium (Figure S7I). We then tested several antiviral drugs experimentally applied for adenoviral conjunctivitis (acyclovir, cidofovir, and nelfinavir) to test their efficacy in blocking the infection.[55] Uniquely, cidofovir could reverse adenoviral infection, making it a potential drug for hAdV8 conjunctivitis (Figures 6G and S7I). The cell-tropism of hAdV8 in the conjunctiva is unknown to date. By staining, we found that both MUC5AC+ goblet cells and MUC5AC− cells (most likely keratinocytes) stained for hAdV8 capsid proteins (Figure 6H), showing that hAdV8 can infect both goblet cells and MUC5AC− cells in the conjunctiva. To map the response of the conjunctival epithelium to hAdV8 infection, we subjected infected and control ALI to bulk RNA sequencing (Figures 6I, S7J, and S7K; Table S6). Beyond the upregulation of genes involved in response to virus and interferon following hAdV8 infection, genes involved in cell cycle were also enriched, including *PCLAF*, *CDK1*, and *CENPM* (Figures 6I, 6J, and S7K). Indeed, KI67+ cells doubled after hAdV8 infection (Figure 6K). Besides, proliferative cells appeared to be located apically rather than only basally (as seen under homeostatic conditions) and displayed an enlarged nucleus, suggesting these were infected by hAdV8 (Figure 6K). Altogether, these data show that viral conjunctivitis can be modeled in this system.

Human conjunctiva organoids engraft orthotopically

Replacement of the human conjunctiva using autologous cell therapy currently does not exist.[56] To repair conjunctival damage, an autograft of healthy conjunctiva from another location in the patient's eye is harvested and used to cover the wound. The sclera underlying the donor site is left bare, and conjunctival scarring often ensues. Consequently, no spare tissue is available for repeated procedures.[57] Conjunctival organoid technology offers a unique potential to restore damaged conjunctiva as it requires less than 1 mm^3 of tissue as starting material.

To test the engraftment capacity of human conjunctiva organoids, we transplanted organoids early after passaging onto the bulbar and fornix conjunctiva of immunodeficient NSG mice that were previously mechanically wounded (Figure 7A). Two days after transplantation, we found human cells engrafted within the recipient conjunctival epithelium, as exemplified by human KRT19 (hKRT19) staining (Figure 7B). Basally located cells had retained expression of the stem cell marker TP63,

some of which expressed KI67, whereas apical cells expressed the keratinocyte marker MUC1 (Figure 7B). After 3 weeks, cells of human origin were present in 11 out of 30 mice (Figures 7C and 7D). 3 eyes showed several engrafted sites and the size of the graft varied from a few cells to ~100 cells (Figures 7E and 7F). Importantly, in these engrafted mice, cells attached to the basement membrane and generated the 3 main cell conjunctival cell types: TP63+ basal cells, MUC1+ keratinocytes, and MUC5AC+ goblet cells (Figure 7C). We concluded that organoids receive adequate cues *in vivo* to trigger the pertinent differentiation cascades. It is worth noting that the human epithelium formed *in vivo* was thicker than the murine epithelium, recapitulating the human conjunctiva characteristics (Figure 7C). Additional engineering of the organoids as a transplantable cell sheet—such as performed for cultured cornea[58]—and transplantation in a rabbit model represents an ongoing next step.

DISCUSSION

Despite its prime importance in maintaining the health of the ocular surface, the conjunctival epithelium has not been studied extensively *in vitro*. The lack of a representative *in vitro* model of the mouse and human conjunctival epithelia has hindered an experimental approach to understand its biology and the development of medications for conjunctival disorders.

Here, we establish adult stem cell-derived mouse and human conjunctival organoids that can be propagated for multiple months. Our medium composition indicates that conjunctival stem cells rely on FGF1 as one key growth factor. FGF1 is expressed in rat conjunctiva[59] and increases corneal wound healing kinetics.[60] Although corneal and conjunctival epithelia are quite distinct in adults, they share a common developmental origin.[3] Thus, similarities in growth factor requirements may not be surprising. We found that WNT signaling was important for both mouse and human conjunctival stem cells. Yet, WNT ligand was required for human organoids to grow, whereas the sole addition of R-spondin 1 was sufficient in the mouse. WNT is a major signaling pathway involved in stem cell maintenance in multiple tissues.[21] Indeed, Wnt has been reported to facilitate conjunctival progenitor propagation on feeder cells.[61] Unexpectedly, although EGF signaling promoted mouse conjunctiva organoid growth, it was detrimental to long-term maintenance of human organoids. Importantly, BMP and TGF-β inhibition were indispensable for organoid maintenance, in line with previous studies showing that BMP inhibition promotes conjunctival stem cell proliferation.[62]

Several *in vivo* models of mouse and human conjunctiva have been developed previously. Yet, it has been notoriously difficult to obtain goblet cells *in vitro*.[63] We find that ALI culture of human organoid-derived conjunctival stem cells strongly improves differentiation toward goblet cells. Under these conditions, the conjunctival epithelium stratifies after ~2 weeks and exhibits ~5 cell layers, similar to the native conjunctiva. Differentiation toward goblet cells, as well as keratinocyte maturation, is clearly visible 17 days after shifting to ALI. Conjunctival cells from various species have been cultured under ALI conditions before without any scaffold, on amniotic membranes, on fibroblasts, or on fibrin. Although conjunctival stratification was largely achieved, human goblet cell differentiation has been limited.[10,64–70] Additional exposure of the ALI cultures to interleukins 4 and 13 further enhances goblet cell differentiation. Indeed, IL-4 and IL-13 are cytokines produced under inflammatory conditions that drive goblet cell hyperplasia in several mucosal tissues, including the lung, the gut, and the conjunctiva.[29,71,72] In the conjunctiva, IL-13 is produced by several immune cell subsets under homeostatic conditions and might thus also participate in maintaining goblet cells in homeostasis.[5,30]

Although most studies have focused on the cornea and the lacrimal gland,[73–76] detailed characterization of the human conjunctival epithelial cell types has been lacking. For example, the conjunctival stem cell identity has remained open, and keratinocytes were often referred to as "epithelial cells."[3] By applying single-cell RNA sequencing to native tissue and cultured conjunctiva, we reveal markers expressed by conjunctival cell types and provide a glimpse of their cellular function. The basal cell compartment drives the observed differences between the conjunctival epithelium and the organoid cultures. Indeed, cells *in vitro* are driven to proliferate and mimic a regenerative response by the growth factor cocktail, whereas the healthy tissue is not in a comparable regenerative state. Furthermore, we show that conjunctival basal cells express markers of basal cells known from other tissues, including *TP63* and *NGFR*.[22,34] Single NGFR+, but not NGFR−, cells can generate organoids that contain both keratinocytes and goblet cells. This solves a long-standing question regarding conjunctival stem cell population(s), their location, and potency.[3] We were able to generate organoids from both palpebral and bulbar conjunctiva. This suggests that conjunctival stem cells are not enriched in a particular location but rather spread throughout the tissue, in agreement with a previous report by Pellegrini et al.[8] In sum, maintenance and repair of the conjunctival epithelium appears to be very similar to that of the skin interfollicular epidermis, where basal cells are located throughout the epidermis and continuously proliferate to replace lost tissue, and to that of the gut epithelium, where proliferative LGR5+ stem cells produce all intestinal differentiated cell types.[77,78]

This single-cell atlas implies that conjunctival keratinocytes may play an additional role in protecting the eye from external insults. Multiple antimicrobial components are found in tears[79,80] and were thought to be only produced by the lacrimal gland.[81] We find these also to be produced by conjunctival keratinocytes. Secretion of antimicrobial peptides is however unlikely to fully protect keratinocytes from bacterial infections.[82] In addition, it is likely that the conjunctival epithelium not only produces the mucin layer of the tear film but also participates in establishing the aqueous layer of the tear film through water release. Indeed, conjunctival keratinocytes express high levels of AQP5, implying water could be apically secreted, which is in line with a previous study.[24] Indeed, we observed that ALI cultures, despite their leak-tightness, were always covered by liquid, implying that liquids are apically secreted.

We report the presence of tuft cells in the human conjunctival epithelium. From single-cell RNA sequencing and histological analyses, these conjunctival tuft cells appear to be very rare, whereas their differentiation can be enhanced by IL-4 and IL-13. Although CHAT-expressing tuft cells were found in the mouse conjunctiva,[37] we did not find any CHAT-expressing

tuft cells in the human conjunctiva atlas. So far, tuft cells have mostly been studied in the gut and in the lung. There, these cells exert functions in type II immune responses and might connect with peripheral nerves.[36] Whether conjunctival tuft cells have the same function(s) remains to be discovered. More generally, this transcriptome atlas uncovers cell states, in particular within the tuft and goblet cell populations, whose relevance should be functionally validated.

Although viruses causing ocular infections have been studied in corneal keratinocytes *in vitro*[51] and in organotypic conjunctival cultures,[70] these are still often studied in other *in vitro* contexts than the ocular surface.[83] We establish a human ocular infection model for HSV1 and hAdV8. hAdV8 is the adenovirus subtype that causes most viral conjunctivitis and is highly contagious.[44] So far, no drug has been approved to treat adenoviral conjunctivitis. In conjunctival ALI, we found that viral replication was inhibited by cidofovir for hAdV8, as seen in a previous trial on adenoviral keratoconjunctivitis,[84] and by acyclovir for HSV1.[85–87] We confirm that SARS-CoV-2 can infect the conjunctival epithelium—similar to a recently described conjunctival organotypic model[70]—consistent with previous studies that found SARS-CoV-2 can cause conjunctivitis.[45,88] Overall, human organoid-derived ALI cultures represent a unique platform to study viral and potentially bacterial infections of the ocular surface and to test relevant drugs.

Taken together, we describe mouse and human conjunctiva organoids and shed light on aspects of conjunctival homeostasis, including stem cell identity and keratinocyte function. This platform may be used to study various ocular diseases in a patient-specific manner, including ocular malignancies, drug toxicity, and viral and bacterial infections. It may also open novel avenues for cell therapy of the conjunctival epithelium.

Limitations of the study

Although adult stem cell-derived organoids represent key aspects of the tissues from which they derive, they are cultured under artificial conditions and by definition present a reductionist version of the tissue under study. Specifically, blood vessels, nerves, stromal cells, and immune cells are absent in these organoids. Thus, any finding in organoids must be verified in primary tissues, preferably *in vivo*.

STAR★METHODS

Detailed methods are provided in the online version of this paper and include the following:

SUPPLEMENTAL INFORMATION

Supplemental information can be found online at https://doi.org/10.1016/j.stem.2023.12.008.

ACKNOWLEDGMENTS

We are grateful to all patients and donors that agreed to participate in the study. We thank Anko de Graaf from the Hubrecht Imaging Center (HIC), Reinier van der Linden, Stefan van Elst, and Anita Pfauth from the FACS facility of the Hubrecht Institute, the animal caretakers of the mouse facility of the Hubrecht Institute, Single Cell Discoveries for sequencing services, the single-cell genomics facility of the Prinses Maxima Center (Utrecht, NL) for the 10x Genomics support, in particular Thanasis Margaritis, Aleksandra Balwierz, and Tito Candelli. We thank Prashant Desai for providing HSV1-tdTomato, Rosemary Millen and Cayetano Pleguezuelos-Manzano for help with FACS, Carola Ammerlaan for help with culturing, Stieneke van den Brink for the production of R-spondin 1 conditioned-medium and Arianne van Velthoven for logistical help. Part of this work was also supported by A*STAR SIgN core fund and BMRC Central Research Fund (UIBR).

AUTHOR CONTRIBUTIONS

M.B.-H. and H.C. conceived and designed the project. M.B.-H. performed and analyzed most experiments and analyzed mouse bulk and human single-cell RNA sequencing data. M.B.-H., J.K., and H.B. performed histology experiments. Z.M. performed and analyzed mass spectrometry analysis, supervised by W.W. M.M.L. performed and analyzed SARS-CoV-2 experiments. A.G. analyzed virus bulk RNA sequencing. C.L.-I., W.J.v.d.W., and P.J.P. performed and analyzed electron microscopy experiments. N.Y. and M.Y. provided hAdV8. J.H.v.E. assisted in writing ethical approvals for mouse experiments. J.K. performed animal experiments. M.B.-H. and J.K. analyzed animal experiments. V.L.S.L. and M.M.D. provided advice to perform the animal experiments. M.M.D., R.K., and S.M.I. provided access to patient

samples. C.L.-I., P.J.P., B.L.H., and H.C. supervised the study and acquired funding. M.B.-H. and H.C. wrote the manuscript with input from all authors.

DECLARATION OF INTERESTS

H.C. is the head of Pharma Research and Early Development at Roche, Basel and holds several patents related to organoid technology. M.B.-H. and H.C. are inventors on a filed patent application related to this work.

Received: July 11, 2023
Revised: September 14, 2023
Accepted: December 11, 2023
Published: January 11, 2024

REFERENCES

1. Diebold, Y., and García-Posadas, L. (2021). Is the Conjunctiva a Potential Target for Advanced Therapy Medicinal Products? Pharmaceutics *13*, 1140.
2. Pflugfelder, S.C., and Stern, M.E. (2020). Biological functions of tear film. Exp. Eye Res. *197*, 108115.
3. Ramos, T., Scott, D., and Ahmad, S. (2015). An update on ocular surface epithelial stem cells: cornea and conjunctiva. Stem Cells Int. *2015*, 601731.
4. Cursiefen, C. (2007). Immune privilege and angiogenic privilege of the cornea. Chem. Immunol. Allergy *92*, 50–57.
5. Alam, J., Yazdanpanah, G., Ratnapriya, R., Borcherding, N., de Paiva, C.S., Li, D., and Pflugfelder, S.C. (2022). Single-cell transcriptional profiling of murine conjunctival immune cells reveals distinct populations expressing homeostatic and regulatory genes. Mucosal Immunol. *15*, 620–628.
6. Mantelli, F., Massaro-Giordano, M., Macchi, I., Lambiase, A., and Bonini, S. (2013). The cellular mechanisms of dry eye: from pathogenesis to treatment. J. Cell. Physiol. *228*, 2253–2256.
7. Clayton, J.A. (2018). Dry eye. N. Engl. J. Med. *378*, 2212–2223.
8. Pellegrini, G., Golisano, O., Paterna, P., Lambiase, A., Bonini, S., Rama, P., and De Luca, M. (1999). Location and clonal analysis of stem cells and their differentiated progeny in the human ocular surface. J. Cell Biol. *145*, 769–782.
9. García-Posadas, L., Arranz-Valsero, I., López-García, A., Soriano-Romaní, L., and Diebold, Y. (2013). A new human primary epithelial cell culture model to study conjunctival inflammation. Invest. Ophthalmol. Vis. Sci. *54*, 7143–7152.
10. García-Posadas, L., Soriano-Romaní, L., López-García, A., and Diebold, Y. (2017). An engineered human conjunctival-like tissue to study ocular surface inflammatory diseases. PLoS One *12*, e0171099.
11. Ang, L.P.K., Tan, D.T.H., Beuerman, R.W., and Lavker, R.M. (2004). Development of a conjunctival epithelial equivalent with improved proliferative properties using a multistep serum-free culture system. Invest. Ophthalmol. Vis. Sci. *45*, 1789–1795.
12. Risse Marsh, B.C., Massaro-Giordano, M., Marshall, C.M., Lavker, R.M., and Jensen, P.J. (2002). Initiation and characterization of keratinocyte cultures from biopsies of normal human conjunctiva. Exp. Eye Res. *74*, 61–69.
13. Shatos, M.A., Rios, J.D., Tepavcevic, V., Kano, H., Hodges, R., and Dartt, D.A. (2001). Isolation, characterization, and propagation of rat conjunctival goblet cells in vitro. Invest. Ophthalmol. Vis. Sci. *42*, 1455–1464.
14. Nomi, K., Hayashi, R., Ishikawa, Y., Kobayashi, Y., Katayama, T., Quantock, A.J., and Nishida, K. (2021). Generation of functional conjunctival epithelium, including goblet cells, from human iPSCs. Cell Rep. *34*, 108715.
15. Fuchs, E., and Green, H. (1981). Regulation of terminal differentiation of cultured human keratinocytes by vitamin A. Cell *25*, 617–625.
16. Sun, T.T., and Green, H. (1977). Cultured epithelial cells of cornea, conjunctiva and skin: absence of marked intrinsic divergence of their differentiated states. Nature *269*, 489–493.
17. Sato, T., Vries, R.G., Snippert, H.J., van de Wetering, M., Barker, N., Stange, D.E., van Es, J.H., Abo, A., Kujala, P., Peters, P.J., et al. (2009). Single Lgr5 stem cells build crypt-villus structures in vitro without a mesenchymal niche. Nature *459*, 262–265.
18. Clevers, H. (2016). Modeling development and disease with organoids. Cell *165*, 1586–1597.
19. Dong, N., Li, W., Lin, H., Wu, H., Li, C., Chen, W., Qin, W., Quyang, L., Wang, H., and Liu, Z. (2009). Abnormal epithelial differentiation and tear film alteration in pinguecula. Invest. Ophthalmol. Vis. Sci. *50*, 2710–2715.
20. Peng, J., Sha, X.Y., Liu, Y., Yang, R.M., and Wen, Y. (2015). Pterygium epithelium abnormal differentiation related to activation of extracellular signal-regulated kinase signaling pathway in vitro. Int. J. Ophthalmol. *8*, 1118–1125.
21. Clevers, H., and Nusse, R. (2012). Wnt/β-catenin signaling and disease. Cell *149*, 1192–1205.
22. Rock, J.R., Onaitis, M.W., Rawlins, E.L., Lu, Y., Clark, C.P., Xue, Y., Randell, S.H., and Hogan, B.L.M. (2009). Basal cells as stem cells of the mouse trachea and human airway epithelium. Proc. Natl. Acad. Sci. USA *106*, 12771–12775.
23. Wolf, J., Hajdu, R.I., Boneva, S., Schlecht, A., Lapp, T., Wacker, K., Agostini, H., Reinhard, T., Auw-Hädrich, C., Schlunck, G., et al. (2021). Characterization of the cellular microenvironment and novel specific biomarkers in pterygia using RNA sequencing. Front. Med. (Lausanne) *8*, 714458.
24. Levin, M.H., and Verkman, A.S. (2004). Aquaporin-dependent water permeation at the mouse ocular surface: in vivo microfluorimetric measurements in cornea and conjunctiva. Invest. Ophthalmol. Vis. Sci. *45*, 4423–4432.
25. Barbosa, F.L., Xiao, Y., Bian, F., Coursey, T.G., Ko, B.Y., Clevers, H., de Paiva, C.S., and Pflugfelder, S.C. (2017). Goblet cells contribute to ocular surface immune tolerance-implications for dry eye disease. Int. J. Mol. Sci. *18*, E978.
26. Gregorieff, A., Stange, D.E., Kujala, P., Begthel, H., van den Born, M., Korving, J., Peters, P.J., and Clevers, H. (2009). The Ets-domain transcription factor Spdef promotes maturation of Goblet and Paneth cells in the intestinal epithelium. Gastroenterology *137*. 1333–45.e1.
27. Chen, S., and Schoen, J. (2019). Air-liquid interface cell culture: from airway epithelium to the female reproductive tract. Reprod. Domest. Anim. *54*, 38–45.
28. Gipson, I.K. (2016). Goblet cells of the conjunctiva: a review of recent findings. Prog. Retin. Eye Res. *54*, 49–63.
29. García-Posadas, L., Hodges, R.R., Diebold, Y., and Dartt, D.A. (2018). Context-dependent regulation of conjunctival goblet cell function by allergic mediators. Sci. Rep. *8*, 12162.
30. De Paiva, C.S., Raince, J.K., McClellan, A.J., Shanmugam, K.P., Pangelinan, S.B., Volpe, E.A., Corrales, R.M., Farley, W.J., Corry, D.B., Li, D.Q., et al. (2011). Homeostatic control of conjunctival mucosal goblet cells by NKT-derived IL-13. Mucosal Immunol. *4*, 397–408.
31. Tukler Henriksson, J., Coursey, T.G., Corry, D.B., De Paiva, C.S., and Pflugfelder, S.C. (2015). IL-13 stimulates proliferation and expression of mucin and immunomodulatory genes in cultured conjunctival goblet cells. Invest. Ophthalmol. Vis. Sci. *56*, 4186–4197.
32. Zhang, Y., Lam, O., Nguyen, M.-T.T., Ng, G., Pear, W.S., Ai, W., Wang, I.J., Kao, W.W.-Y., and Liu, C.Y. (2013). Mastermind-like transcriptional co-activator-mediated Notch signaling is indispensable for maintaining conjunctival epithelial identity. Development *140*, 594–605.
33. Wang, S., Drummond, M.L., Guerrero-Juarez, C.F., Tarapore, E., MacLean, A.L., Stabell, A.R., Wu, S.C., Gutierrez, G., That, B.T., Benavente, C.A., et al. (2020). Single cell transcriptomics of human

epidermis identifies basal stem cell transition states. Nat. Commun. *11*, 4239.

34. Tomellini, E., Lagadec, C., Polakowska, R., and Le Bourhis, X. (2014). Role of p75 neurotrophin receptor in stem cell biology: more than just a marker. Cell. Mol. Life Sci. *71*, 2467–2481.
35. Choreño-Parra, J.A., Thirunavukkarasu, S., Zúñiga, J., and Khader, S.A. (2020). The protective and pathogenic roles of CXCL17 in human health and disease: potential in respiratory medicine. Cytokine Growth Factor Rev. *53*, 53–62.
36. Kotas, M.E., O'Leary, C.E., and Locksley, R.M. (2023). Tuft cells: context- and tissue-specific programming for a conserved cell lineage. Annu. Rev. Pathol. *18*, 311–335.
37. Wiederhold, S., Papadakis, T., Chubanov, V., Gudermann, T., Krasteva-Christ, G., and Kummer, W. (2015). A novel cholinergic epithelial cell with chemosensory traits in the murine conjunctiva. Int. Immunopharmacol. *29*, 45–50.
38. Gerbe, F., Sidot, E., Smyth, D.J., Ohmoto, M., Matsumoto, I., Dardalhon, V., Cesses, P., Garnier, L., Pouzolles, M., Brulin, B., et al. (2016). Intestinal epithelial tuft cells initiate type 2 mucosal immunity to helminth parasites. Nature *529*, 226–230.
39. Gracz, A.D., Samsa, L.A., Fordham, M.J., Trotier, D.C., Zwarycz, B., Lo, Y.H., Bao, K., Starmer, J., Raab, J.R., Shroyer, N.F., et al. (2018). SOX4 promotes ATOH1-independent intestinal secretory differentiation toward tuft and enteroendocrine fates. Gastroenterology *155*, 1508–1523.e10.
40. Junttila, I.S. (2018). Tuning the cytokine responses: an update on interleukin (IL)-4 and IL-13 receptor complexes. Front. Immunol. *9*, 888.
41. Izuhara, K., Nunomura, S., Nanri, Y., Ogawa, M., Ono, J., Mitamura, Y., and Yoshihara, T. (2017). Periostin in inflammation and allergy. Cell. Mol. Life Sci. *74*, 4293–4303.
42. Saint-Criq, V., Guequén, A., Philp, A.R., Villanueva, S., Apablaza, T., Fernández-Moncada, I., Mansilla, A., Delpiano, L., Ruminot, I., Carrasco, C., et al. (2022). Inhibition of the sodium-dependent HCO3-transporter SLC4A4, produces a cystic fibrosis-like airway disease phenotype. eLife *11*, e75871.
43. Gorrieri, G., Scudieri, P., Caci, E., Schiavon, M., Tomati, V., Sirci, F., Napolitano, F., Carrella, D., Gianotti, A., Musante, I., et al. (2016). Goblet cell hyperplasia requires high bicarbonate transport to support mucin release. Sci. Rep. *6*, 36016.
44. Akello, J.O., Kamgang, R., Barbani, M.T., Suter-Riniker, F., Leib, S.L., and Ramette, A. (2020). Epidemiology of human adenoviruses: A 20-year retrospective observational study in hospitalized patients in Bern, Switzerland. Clin. Epidemiol. *12*, 353–366.
45. Al-Namaeh, M. (2021). COVID-19 and conjunctivitis: a meta-analysis. Ther. Adv. Ophthalmol. *13*, 25158414211003368.
46. Hidalgo, F., Melón, S., de Oña, M., Do Santos, V., Martínez, A., Cimadevilla, R., and Rodríguez, M. (1998). Diagnosis of herpetic keratoconjunctivitis by nested polymerase chain reaction in human tear film. Eur. J. Clin. Microbiol. Infect. Dis. *17*, 120–123.
47. Hutama, S.A., Alkaff, F.F., Intan, R.E., Maharani, C.D., Indriaswati, L., and Zuhria, I. (2022). Recurrent keratoconjunctivitis as the sole manifestation of COVID-19 infection: A case report. Eur. J. Ophthalmol. *32*, NP17–NP21.
48. Labib, B.A., Minhas, B.K., and Chigbu, D.I. (2020). Management of adenoviral keratoconjunctivitis: challenges and solutions. Clin. Ophthalmol. *14*, 837–852.
49. Connolly, S.A., Jardetzky, T.S., and Longnecker, R. (2021). The structural basis of herpesvirus entry. Nat. Rev. Microbiol. *19*, 110–121.
50. Hoffmann, M., Kleine-Weber, H., Schroeder, S., Krüger, N., Herrler, T., Erichsen, S., Schiergens, T.S., Herrler, G., Wu, N.H., Nitsche, A., et al. (2020). SARS-CoV-2 cell entry depends on ACE2 and TMPRSS2 and is blocked by a clinically proven protease inhibitor. Cell *181*, 271–280.e8.
51. Storm, R.J., Persson, B.D., Skalman, L.N., Frängsmyr, L., Lindström, M., Rankin, G., Lundmark, R., Domellöf, F.P., and Arnberg, N. (2017). Human adenovirus Type 37 uses αVβ1 and α3β1 integrins for infection of human corneal cells. J. Virol. *91*. e02019–e02016.
52. Etienne, L., Joshi, P., Dingle, L., Huang, E., Grzesik, P., and Desai, P.J. (2017). Visualization of herpes simplex virus type 1 virions using fluorescent colors. J. Virol. Methods *241*, 46–51.
53. Skevaki, C.L., Galani, I.E., Pararas, M.V., Giannopoulou, K.P., and Tsakris, A. (2011). Treatment of viral conjunctivitis with antiviral drugs. Drugs *71*, 331–347.
54. Yawata, N., and Yawata, M. (2022). Assessing the response of human NK cell subsets to infection by clinically isolated virus strains. Methods Mol. Biol. *2463*, 205–220.
55. Dodge, M.J., MacNeil, K.M., Tessier, T.M., Weinberg, J.B., and Mymryk, J.S. (2021). Emerging antiviral therapeutics for human adenovirus infection: recent developments and novel strategies. Antiviral Res. *188*, 105034.
56. Cursiefen, C., Cordeiro, F., Cunha-Vaz, J., Wheeler-Schilling, T., and Scholl, H.P.N.; EVI; Steering Board (2019). O.B. of T. unmet needs in ophthalmology: a European vision institute-consensus roadmap 2019–2025. ORE *62*, 123–133.
57. Shahraki, T., Arabi, A., and Feizi, S. (2021). Pterygium: an update on pathophysiology, clinical features, and management. Ther. Adv. Ophthalmol. *13*, 25158414211020152.
58. Rama, P., Matuska, S., Paganoni, G., Spinelli, A., De Luca, M., and Pellegrini, G. (2010). Limbal stem-cell therapy and long-term corneal regeneration. N. Engl. J. Med. *363*, 147–155.
59. Noji, S., Matsuo, T., Koyama, E., Yamaai, T., Nohno, T., Matsuo, N., and Taniguchi, S. (1990). Expression pattern of acidic and basic fibroblast growth factor genes in adult rat eyes. Biochem. Biophys. Res. Commun. *168*, 343–349.
60. Fredj-Reygrobellet, D., Plouet, J., Delayre, T., Baudouin, C., Bourret, F., and Lapalus, P. (1987). Effects of aFGF and bFGF on wound healing in rabbit corneas. Curr. Eye Res. *6*, 1205–1209.
61. Schrader, S., O'Callaghan, A.R., Tuft, S.J., Beaconsfield, M., Geerling, G., and Daniels, J.T. (2014). Wnt signalling in an in vitro niche model for conjunctival progenitor cells. J. Tissue Eng. Regen. Med. *8*, 969–977.
62. Huang, J., Dattilo, L.K., Rajagopal, R., Liu, Y., Kaartinen, V., Mishina, Y., Deng, C.X., Umans, L., Zwijsen, A., Roberts, A.B., et al. (2009). FGF-regulated BMP signaling is required for eyelid closure and to specify conjunctival epithelial cell fate. Development *136*, 1741–1750.
63. García-Posadas, L., and Diebold, Y. (2020). Three-dimensional human cell culture models to study the pathophysiology of the anterior eye. Pharmaceutics *12*, 1215.
64. Tsai, R.J., Ho, Y.S., and Chen, J.K. (1994). The effects of fibroblasts on the growth and differentiation of human bulbar conjunctival epithelial cells in an in vitro conjunctival equivalent. Invest. Ophthalmol. Vis. Sci. *35*, 2865–2875.
65. Meller, D., and Tseng, S.C. (1999). Conjunctival epithelial cell differentiation on amniotic membrane. Invest. Ophthalmol. Vis. Sci. *40*, 878–886.
66. Paladino, G., Marino, C., La Terra Mulè, S., Civiale, C., Rusciano, D., and Enea, V. (2004). Cytokeratin expression in primary epithelial cell culture from bovine conjunctiva. Tissue Cell *36*, 323–332.
67. Chung, S.H., Lee, J.H., Yoon, J.H., Lee, H.K., and Seo, K.Y. (2007). Multilayered culture of primary human conjunctival epithelial cells producing MUC5AC. Exp. Eye Res. *85*, 226–233.
68. Seo, K.Y., Jeon, S., Choi, S.H., and Chung, S.H. (2011). Niflumic acid reduces histamine-induced MUC5AC expression in human conjunctival epithelial cells. Ophthal. Res. *46*, 181–186.
69. Lee, J., Jun, E.J., Sunwoo, J.H., Kim, E.S., Kim, J.H., Kim, J.Y., Kim, M.J., Kim, Y.K., Lee, H., and Tchah, H. (2011). An ex vivo model of Coxsackievirus infection using multilayered human conjunctival epithelial cells. Graefes Arch. Clin. Exp. Ophthalmol. *249*, 1327–1332.
70. Jackson, R.M., Hatton, C.F., Spegarova, J.S., Georgiou, M., Collin, J., Stephenson, E., Verdon, B., Haq, I.J., Hussain, R., Coxhead, J.M.,

et al. (2022). Conjunctival epithelial cells resist productive SARS-CoV-2 infection. Stem Cell Rep. *17*, 1699–1713.

71. Gour, N., and Wills-Karp, M. (2015). IL-4 and IL-13 signaling in allergic airway disease. Cytokine *75*, 68–78.
72. McKenzie, G.J., Bancroft, A., Grencis, R.K., and McKenzie, A.N.J. (1998). A distinct role for interleukin-13 in Th2-cell-mediated immune responses. Curr. Biol. *8*, 339–342.
73. Aakalu, V.K., Parameswaran, S., Maienschein-Cline, M., Bahroos, N., Shah, D., Ali, M., and Krishnakumar, S. (2017). Human lacrimal gland gene expression. PLoS One *12*, e0169346.
74. Guo, Z.H., Jia, Y.Y.S., Zeng, Y.M., Li, Z.F., and Lin, J.S. (2021). Transcriptome analysis identifies the differentially expressed genes related to the stemness of limbal stem cells in mice. Gene *775*, 145447.
75. Català, P., Groen, N., Dehnen, J.A., Soares, E., van Velthoven, A.J.H., Nuijts, R.M.M.A., Dickman, M.M., and LaPointe, V.L.S. (2021). Single cell transcriptomics reveals the heterogeneity of the human cornea to identify novel markers of the limbus and stroma. Sci. Rep. *11*, 21727.
76. Collin, J., Queen, R., Zerti, D., Bojic, S., Dorgau, B., Moyse, N., Molina, M.M., Yang, C., Dey, S., Reynolds, G., et al. (2021). A single cell atlas of human cornea that defines its development, limbal progenitor cells and their interactions with the immune cells. Ocul. Surf. *21*, 279–298.
77. Solanas, G., and Benitah, S.A. (2013). Regenerating the skin: a task for the heterogeneous stem cell pool and surrounding niche. Nat. Rev. Mol. Cell Biol. *14*, 737–748.
78. Barker, N., van Es, J.H., Kuipers, J., Kujala, P., van den Born, M., Cozijnsen, M., Haegebarth, A., Korving, J., Begthel, H., Peters, P.J., et al. (2007). Identification of stem cells in small intestine and colon by marker gene Lgr5. Nature *449*, 1003–1007.
79. Perumal, N., Funke, S., Wolters, D., Pfeiffer, N., and Grus, F.H. (2015). Characterization of human reflex tear proteome reveals high expression of lacrimal proline-rich protein 4 (PRR4). Proteomics *15*, 3370–3381.
80. Perumal, N., Funke, S., Pfeiffer, N., and Grus, F.H. (2016). Proteomics analysis of human tears from aqueous-deficient and evaporative dry eye patients. Sci. Rep. *6*, 29629.
81. Bannier-Hélaouët, M., Post, Y., Korving, J., Trani Bustos, M., Gehart, H., Begthel, H., Bar-Ephraim, Y.E., van der Vaart, J., Kalmann, R., Imhoff, S.M., et al. (2021). Exploring the human lacrimal gland using organoids and single-cell sequencing. Cell Stem Cell *28*, 1221–1232.e7.
82. Gallo, R.L., and Hooper, L.V. (2012). Epithelial antimicrobial defence of the skin and intestine. Nat. Rev. Immunol. *12*, 503–516.
83. Toth, K., Hussein, I.T.M., Tollefson, A.E., Ying, B., Spencer, J.F., Eagar, J., James, S.H., Prichard, M.N., Wold, W.S.M., and Bowlin, T.L. (2020). Filociclovir is a potent in vitro and in vivo inhibitor of human adenoviruses. Antimicrob. Agents Chemother. *64*, e01299-20.
84. Hillenkamp, J., Reinhard, T., Ross, R.S., Böhringer, D., Cartsburg, O., Roggendorf, M., De Clercq, E., Godehardt, E., and Sundmacher, R. (2002). The effects of cidofovir 1% with and without cyclosporin A 1% as a topical treatment of acute adenoviral keratoconjunctivitis: a controlled clinical pilot study. Ophthalmology *109*, 845–850.
85. Romanowski, E.G., Hussein, I.T.M., Cardinale, S.C., Butler, M.M., Morin, L.R., Bowlin, T.L., Yates, K.A., Shanks, R.M.Q., and Kowalski, R.P. (2021). Filociclovir is an active antiviral agent against ocular adenovirus isolates in vitro and in the Ad5/NZW rabbit ocular model. Pharmaceuticals (Basel) *14*, 294.
86. Driehuis, E., Kolders, S., Spelier, S., Lõhmussaar, K., Willems, S.M., Devriese, L.A., de Bree, R., de Ruiter, E.J., Korving, J., Begthel, H., et al. (2019). Oral mucosal organoids as a potential platform for personalized cancer therapy. Cancer Discov. *9*, 852–871.
87. Lõhmussaar, K., Oka, R., Espejo Valle-Inclan, J., Smits, M.H.H., Wardak, H., Korving, J., Begthel, H., Proost, N., van de Ven, M., Kranenburg, O.W., et al. (2021). Patient-derived organoids model cervical tissue dynamics and viral oncogenesis in cervical cancer. Cell Stem Cell *28*, 1380–1396.e6.
88. Eriksen, A.Z., Møller, R., Makovoz, B., Uhl, S.A., tenOever, B.R., and Blenkinsop, T.A. (2021). SARS-CoV-2 infects human adult donor eyes and hESC-derived ocular epithelium. Cell Stem Cell *28*, 1205–1220.e7.
89. Pleguezuelos-Manzano, C., Puschhof, J., van den Brink, S., Geurts, V., Beumer, J., and Clevers, H. (2020). Establishment and culture of human intestinal organoids derived from adult stem cells. Curr. Protoc. Immunol. *130*, e106.
90. Ran, F.A., Hsu, P.D., Wright, J., Agarwala, V., Scott, D.A., and Zhang, F. (2013). Genome engineering using the CRISPR-Cas9 system. Nat. Protoc. *8*, 2281–2308.
91. Travaglini, K.J., Nabhan, A.N., Penland, L., Sinha, R., Gillich, A., Sit, R.V., Chang, S., Conley, S.D., Mori, Y., Seita, J., et al. (2020). A molecular cell atlas of the human lung from single-cell RNA sequencing. Nature *587*, 619–625.
92. Elmentaite, R., Kumasaka, N., Roberts, K., Fleming, A., Dann, E., King, H.W., Kleshchevnikov, V., Dabrowska, M., Pritchard, S., Bolt, L., et al. (2021). Cells of the human intestinal tract mapped across space and time. Nature *597*, 250–255.
93. Kumar, V., Ramnarayanan, K., Sundar, R., Padmanabhan, N., Srivastava, S., Koiwa, M., Yasuda, T., Koh, V., Huang, K.K., Tay, S.T., et al. (2022). Single-cell atlas of lineage states, tumor microenvironment, and subtype-specific expression programs in gastric cancer. Cancer Discov. *12*, 670–691.
94. Corman, V.M., Landt, O., Kaiser, M., Molenkamp, R., Meijer, A., Chu, D.K., Bleicker, T., Brünink, S., Schneider, J., Schmidt, M.L., et al. (2020). Detection of 2019 novel coronavirus (2019-nCoV) by real-time RT-PCR. Euro Surveill. *25*, 2000045.
95. Miura-Ochiai, R., Shimada, Y., Konno, T., Yamazaki, S., Aoki, K., Ohno, S., Suzuki, E., and Ishiko, H. (2007). Quantitative detection and rapid identification of human adenoviruses. J. Clin. Microbiol. *45*, 958–967.
96. Hao, Y., Hao, S., Andersen-Nissen, E., Mauck, W.M., Zheng, S., Butler, A., Lee, M.J., Wilk, A.J., Darby, C., Zager, M., et al. (2021). Integrated analysis of multimodal single-cell data. Cell *184*, 3573–3587.e29.
97. Stuart, T., Butler, A., Hoffman, P., Hafemeister, C., Papalexi, E., Mauck, W.M., Hao, Y., Stoeckius, M., Smibert, P., and Satija, R. (2019). Comprehensive integration of single-cell data. Cell *177*, 1888–1902.e21.
98. Li, H. (2011). A statistical framework for SNP calling, mutation discovery, association mapping and population genetical parameter estimation from sequencing data. Bioinformatics *27*, 2987–2993.
99. Smith, T., Heger, A., and Sudbery, I. (2017). UMI-tools: modeling sequencing errors in Unique Molecular Identifiers to improve quantification accuracy. Genome Res. *27*, 491–499.
100. Heaton, H., Talman, A.M., Knights, A., Imaz, M., Gaffney, D.J., Durbin, R., Hemberg, M., and Lawniczak, M.K.N. (2020). Souporcell: robust clustering of single-cell RNA-seq data by genotype without reference genotypes. Nat. Methods *17*, 615–620.
101. Love, M.I., Huber, W., and Anders, S. (2014). Moderated estimation of fold change and dispersion for RNA-seq data with DESeq2. Genome Biol. *15*, 550.
102. Young, M.D., Wakefield, M.J., Smyth, G.K., and Oshlack, A. (2010). Gene ontology analysis for RNA-seq: accounting for selection bias. Genome Biol. *11*, R14.
103. Yu, G., Wang, L.G., Han, Y., and He, Q.Y. (2012). clusterProfiler: an R package for comparing biological themes among gene clusters. OMICS A J. Integr. Biol. *16*, 284–287.
104. Zhu, L.J., Gazin, C., Lawson, N.D., Pagès, H., Lin, S.M., Lapointe, D.S., and Green, M.R. (2010). ChIPpeakAnno: a Bioconductor package to annotate ChIP-seq and ChIP-chip data. BMC Bioinformatics *11*, 237.
105. Andersson-Rolf, A., Mustata, R.C., Merenda, A., Kim, J., Perera, S., Grego, T., Andrews, K., Tremble, K., Silva, J.C.R., Fink, J., et al. (2017). One-step generation of conditional and reversible gene knockouts. Nat. Methods *14*, 287–289.

106. Fujii, M., Matano, M., Nanki, K., and Sato, T. (2015). Efficient genetic engineering of human intestinal organoids using electroporation. Nat. Protoc. *10*, 1474–1485.

107. GeurtsvanKessel, C.H., Geers, D., Schmitz, K.S., Mykytyn, A.Z., Lamers, M.M., Bogers, S., Scherbeijn, S., Gommers, L., Sablerolles, R.S.G., Nieuwkoop, N.N., et al. (2022). Divergent SARS-CoV-2 Omicron-reactive T and B cell responses in COVID-19 vaccine recipients. Sci. Immunol. *7*, eabo2202.

108. Lamers, M.M., Mykytyn, A.Z., Breugem, T.I., Wang, Y., Wu, D.C., Riesebosch, S., van den Doel, P.B., Schipper, D., Bestebroer, T., Wu, N.C., et al. (2021). Human airway cells prevent SARS-CoV-2 multibasic cleavage site cell culture adaptation. eLife *10*, e66815.

109. Lamers, M.M., Mykytyn, A.Z., Breugem, T.I., Groen, N., Knoops, K., Schipper, D., van Acker, R., van den Doel, P.B., Bestebroer, T., Koopman, C.D., et al. (2022). SARS-CoV-2 Omicron efficiently infects human airway, but not alveolar epithelium. https://doi.org/10.1101/2022.01.19.476898.

STAR★METHODS

KEY RESOURCES TABLE

REAGENT or RESOURCE	SOURCE	IDENTIFIER
Antibodies		
Anti-PAX6	Biolegend	90131, RRID: AB_2565003
Anti-LCN2	R&D Systems	AF1757, RRID: AB_354974
Anti-GAPDH	Labned	LN2100751
Anti-MUC5AC	Thermo Fisher scientific	MA5-12175, RRID: AB_10983421
Anti-MUC1	Abcam	ab15481, RRID: AB_301891
Anti-AQP5	Origene	TA321387
Anti-mouse KRT19	Cell Signalling Technologies	13092, RRID: AB_2722626
Anti-human KRT19	Cell Signalling Technologies	4558S, RRID: AB_2133455
Anti-AVIL	Sigma-Aldrich	HPA058864, RRID: AB_2683838
Anti-WFDC2	LSBio	LS-C175346
Anti-TFF3	Atlas Antibodies	HPA035464, RRID: AB_2674636
Anti-TP63	Abcam	ab735, RRID: AB_305870
Anti-KI67	eBiosciences	14-5698-82, RRID: AB_10854564
Anti-mouse KI67	Abcam	ab16667, RRID: AB_302459
Anti-human KI67	BD Pharmingen	550609, RRID: AB_393778
Anti-SLC4A4	Atlas Antibodies	HPA035628, RRID: AB_2674708
Anti-human nucleoli	Abcam	ab-190710
Anti-SARS-CoV nucleoprotein	Sino Biological	40588-T62
Anti-adenovirus FITC-conjugated	Millipore	AB1056F, RRID: AB_90204
PE anti-human NGFR	Biolegend	345106, RRID: AB_2152647
Alexa Fluor 488 donkey anti-rabbit	Thermo Fisher scientific	A21206, RRID: AB_2535792
Alexa Fluor 568 donkey anti-mouse	Thermo Fisher scientific	A10037, RRID: AB_2534013
Alexa Fluor 568 donkey anti-rabbit	Thermo Fisher scientific	A10042, RRID: AB_2534017
Alexa Fluor 568 donkey anti-goat	Thermo Fisher scientific	A11057, RRID: AB_2534104
Alexa Fluor 555 goat anti-rat	Thermo Fisher scientific	A21434, RRID: AB_2535855
Phalloidin–Atto 647N	Sigma-Aldrich	65906
CruzFluor647-labeled phalloidin	Santa Cruz	sc-363797
Rabbit anti-goat IgG(H+L)-UNLB	Southern Biotech	6160-01, RRID: AB_2796227
Rabbit Anti-Rat IgG(H+L), Human ads-UNLB	Southern Biotech	6185-01, RRID: AB_2796259
Rabbit anti-mouse HRP	Dako	P0161, RRID: AB_2687969
Rabbit anti-goat HRP	Dako	P044901-2
Swine anti-rabbit HRP	Dako	P021702-2
Streptavidin peroxidase	Thermo Fisher scientific	TS-125-HR
EnVision+/HRP mouse	Agilent	K400111-2
EnVision+/HRP rabbit	Agilent	K400311-2
Biological Samples		
Human conjunctiva tissue	Utrecht Medical Center	TCbio protocol 18-740
Human conjunctiva tissue	Maastricht UMC+	METC protocol 2021-2732
Human conjunctiva tissue	ETB-BISLIFE cornea bank	N/A
Calu-3 cells	ATCC	HTB55
VeroE6 cells	ATCC	CRL1586
Mouse conjunctiva tissue for organoids	Hubrecht Institute	N/A

(*Continued on next page*)

Continued

REAGENT or RESOURCE	SOURCE	IDENTIFIER
Surplus mouse conjunctiva tissue (C57/Bl6 mice)	Hubrecht Institute	N/A
NSG mice	Hubrecht Institute	Project license:AVD8010020209924
Chemicals, Peptides, and Recombinant Proteins		
DNase I	Sigma Aldrich	DN25
Trypsin/EDTA 0.5 % phenol red-free	Thermo Fisher scientific	15400054
Dispase	Thermo Fisher scientific	17105-041
PVDF membrane	Millipore	IPVH00010
Complete mini protease inhibitor cocktail tablets	Roche	11836170001
CellTiterGlo 3D	Promega	G9683
CellBanker I	Amsbio	11888
Fetal bovine serum	Sigma Aldrich	F7524
Red blood cell lysis buffer	Sigma Aldrich	11814389001
Opti-MEM I	Thermo Fisher scientific	31985070
Advanced DMEM/F12	Thermo Fisher scientific	12634-010
B-27 Supplement	Thermo Fisher scientific	17504044
GlutaMAX	Thermo Fisher scientific	35050061
HEPES	Thermo Fisher scientific	15630080
Penicillin-Streptomycin	Thermo Fisher scientific	15140122
Wnt surrogate	U-Protein Express	Custom order
Noggin conditioned medium	U-Protein Express	Custom order
R-spondin 3 conditioned medium	U-Protein Express	Custom order
R-spondin 1 conditioned medium	Pleguezuelos-Manzano et al.[89]	N/A
N-Acetyl-L-cysteine	Sigma-Aldrich	A9165
EGF	Peprotech	AF-100-15
FGF1	Peprotech	100-17A
FGF10	Peprotech	100-26
Forskolin	Tocris	1099
A83-01	Tocris	2939
Y-27632 dihydrochloride	Abmole	M1817
DAPT	Sigma-Aldrich	D5942
IL-4	Peprotech	200-04
IL-13	Peprotech	200-13
Primocin	Invivogen	ant-pm-2
Hygromycin	Invivogen	ant-hg-2
Acyclovir	Sigma Aldrich	PHR1254
Cidofovir	Sigma Aldrich	C5874
Nelfinavir	Sigma Aldrich	PZ0013
Cultrex Basement Membrane Extract (BME), Growth Factor Reduced, Type 2	R&D Systems, Bio-Techne	3533-001-02
Rat tail collagen I	Thermo Fisher scientific	A1048301
Normal goat serum	Thermo Fisher scientific	50197Z
DAPI	Thermo Fisher scientific	D1306
DRAQ5	Biostatus	62251
ProLong Gold Antifade Mountant with DAPI	Thermo Fisher scientific	P36935
SYBR Green	Bio-Rad	1725270
GoScript Reverse Transcriptase	Promega	A5003
Random Primers	Promega	C1181
QuickExtract	Lucigen	QE09050

(*Continued on next page*)

Continued

REAGENT or RESOURCE	SOURCE	IDENTIFIER
BSA	MP biomedicals	160069
Triton X-100	Sigma-Aldrich	X100-100ML
Pertex	Klinipath	AM-08010
pSpCas9(BB)-2A-GFP gRNA cloning reagents	Ran et al.[90]	N/A
BTXpress solution	BTX	45-0805
DTT	Sigma Aldrich	D0632
Lysyl endopeptidase (Lys C)	Wako Chemicals GmbH	129-05061
Reversed-phase C18 1cc columns	Waters Corporation	WAT054925
Trypsin	Sigma Aldrich	T1426
Fibrin TISSEEL	Baxter	1506079
Critical Commercial Assays		
RNeasy Mini Kit	QIAGEN	74104
QIAquick PCR Purification Kit	QIAGEN	28104
Quick-DNA Microprep kit	Zymogen	ZY-D3020
Chromium 3' Gene Expression solution v3.1	10x Genomics	PN-120237
TruSeq Stranded mRNA kit	Illumina	N/A
pJet cloning kit	Thermo Fisher scientific	K1232
Miniprep DNA isolation kit	Thermo Fisher scientific	K210003
Midiprep DNA isolation kit	Thermo Fisher scientific	K210005
Micro BCA™ Protein Assay Kit	Bio-Rad	23235
4-15% Mini-PROTEAN precast protein gel 10-well 30 μL	Bio-Rad	4561083
ECL Prime Western blotting detection reagent	GE Healthcare Life Sciences	RPN2232
Deposited Data		
Raw and processed mouse conjunctiva bulk mRNA sequencing data	This paper	GEO: GSE205926
Raw and processed human conjunctiva single-cell mRNA sequencing data	This paper	GEO: GSE242382
Raw and processed human conjunctiva infected with HSV1 and hAdV8 bulk mRNA sequencing data	This paper	GEO: GSE205925
Processed human lung single-cell atlas	Travaglini et al.[91]	https://www.synapse.org/#!Synapse:syn21041850
Processed human gut single-cell atlas: epithelial cells	Elmentaite et al.[92]	https://www.gutcellatlas.org/
Processed human stomach single-cell atlas	Kumar et al.[93]	GEO: GSE183904
Pterygium and healthy conjunctiva bulk mRNA sequencing data	Wolf et al.[23]	GEO: GSE155776
Raw conjunctival secretome data	This paper	ProteomeXchange: PXD043550
Compiled code used for human single-cell RNA sequencing analysis	This paper	https://github.com/MarieBannier/Conjunctiva
Seurat objects of human conjunctiva single-cell RNA sequencing	This paper	Zenodo: 8403667
Experimental Models: Organisms/Strains		
C57BL/6 mice	Hubrecht Institute	N/A
NOD Scid Gamma (NSG) mice	Hubrecht Institute	N/A
HSV1-tdTomato	Etienne et al.[52]	N/A
hAdV8	This paper	N/A
SARS-CoV-2 (ancestral strain, 614G)	EVAg	026V-03883
SARS-CoV-2 (Delta variant)	GenBank	OM287123

(*Continued on next page*)

Continued

REAGENT or RESOURCE	SOURCE	IDENTIFIER
Oligonucleotides		
qPCR primers	This paper, Bannier-Hélaouët et al.,[81] and Table S7	N/A
Viral titer primers	This paper, Corman et al.,[94] Lõhmussaar et al.,[87] Miura-Ochiai et al.,[95] and Table S7	N/A
Pax6 KO primers	Bannier-Hélaouët et al.[81] and Table S7	N/A
Software and Algorithms		
CFX manager software	Bio-Rad	N/A
Seurat v3 and v4	Stuart et al. and Hao et al.[96,97]	https://satijalab.org/seurat/index.html
Samtools v1.10	Li[98]	http://www.htslib.org/
umi_tools v1.1.1	Smith et al.[99]	https://github.com/CGATOxford/UMI-tools
CellRanger v7.1.0	10x genomics	https://support.10xgenomics.com/single-cell-gene-expression/software/pipelines/latest/installation
Souporcell	Heaton et al.[100]	https://github.com/wheaton5/souporcell
DESeq2 v1.26.0	Love et al.[101]	https://github.com/mikelove/DESeq2
Goseq	Young et al.[102]	https://rdrr.io/github/nadiadavidson/goseq/
clusterProfiler v3.14.0	Yu et al.[103]	https://github.com/YuLab-SMU/clusterProfiler
ChIPpeakAnno v3.20.0	Zhu et al.[104]	https://rdrr.io/bioc/ChIPpeakAnno/man/
Python	Python	https://www.python.org/
R version 4.1.0	R Core	https://www.r-project.org/
Rstudio	Rstudio	https://rstudio.com/
MaxQuant v2.4.2.0	MaxQuant	https://www.maxquant.org/
Uniprot human database	Uniprot	https://www.uniprot.org/
Perseus v1.6.15.0	Max Planck Institute of Biochemistry	https://maxquant.net/perseus/
GraphPad PRISM 9	GraphPad	N/A
Las X	Leica	N/A
Adobe illustrator	Adobe inc.	N/A
Fiji	NIH, Fiji developers	https://imagej.net/Fiji
Other		
EVOS FL Auto 2 Cell Imaging System	Thermo Fisher scientific	N/A
ImageQuant LAS 4000 ECL western blot imager	GE Healthcare Life Sciences	N/A
LSM700 confocal microscope	Zeiss	N/A
SP8 confocal microscope	Leica	N/A
SP8X confocal microscope	Leica	N/A
DM4000	Leica	N/A
NEPA21 electroporator	Nepagene	N/A
Ultramicrotome Ultracut	Leica	N/A
Tecnai T12 electron microscope	Thermo Fisher scientific	N/A
Eagle 4k*4k CCD camera	Thermo Fisher scientific	N/A
NovaSeq6000	Illumina	N/A
CFX384 Touch Real-Time PCR detection system	Bio-Rad	N/A
Spark multimode microplate reader	Tecan	N/A
12-well suspension plates	Greiner	665102
24-well suspension plates	Greiner	662102

(*Continued on next page*)

Continued

REAGENT or RESOURCE	SOURCE	IDENTIFIER
Thincert cell culture insert for 24 well plates	Greiner	662630
Orbitrap Eclipse Tribrid Mass Spectrometer	Thermo Fisher scientific	N/A
Vanquish Neo UHPLC System	Thermo Fisher scientific	N/A
Easy-Spray PepMap Neo 2 μm C18 75 μm X 500 mm	Thermo Fisher scientific	ES75500PN
FACSFusion	BD Biosciences	N/A
FACSAria	BD Biosciences	N/A
FACSJazz	BD Biosciences	N/A

RESOURCE AVAILABILITY

Lead contact

Further information and requests for resources and reagents should be directed to and will be fulfilled by the Lead Contact, Hans Clevers (h.clevers@hubrecht.eu).

Materials availability

Mouse organoid lines are available upon request with appropriate MTA. There are restrictions to the availability of human organoid lines owing to hospitals ethical regulations.

Data and code availability

- Single-cell and bulk RNA-seq data have been deposited at GEO and are publicly available as of the date of publication. Accession numbers are listed in the key resources table. Proteomics raw data have been deposited to the ProteomeXchange Consortium and are publicly available as of the date of publication. Accession numbers are listed in the key resources table. This paper analyzes existing, publicly available data. These accession numbers for the datasets are listed in the key resources table.
- This paper does not report original code.
- Any additional information required to reanalyze the data reported is available from the lead contact upon request.

EXPERIMENTAL MODEL AND STUDY PARTICIPANT DETAILS

Animals

Mouse conjunctival tissue for organoid derivation was obtained from surplus C57/BL6 mice.

Organoid orthotopic transplantations in 8-16 week-old, 20-35 grams, NOD Scid Gamma (NSG) immunodeficient mouse were conducted under a project license granted by the Dutch government's Central Committee Animal Experimentation (CCD) (HI 21.39-02 (AVD 80100 2020 9924)) and approved by the KNAW-Hubrecht Institute Animal Welfare Body. Males were used for practical reasons of colony maintenance. Mice were housed individually for the first seven days after transplantation to avoid mutual scratching. Past this period, mice were housed collectively. Housing was done in a specific-pathogen-free facility, with unrestricted access to food and water.

Human samples

Human conjunctival samples were leftover material from patients undergoing eyelid surgeries at the University Medical Center Utrecht, the Netherlands (UMCU, donors "U", n = 3), from patients undergoing pterygium removal at the Maastricht University Medical Center, the Netherlands (MUMC+, donors "M", n = 13) or from a donor at the ETB-BISLIFE cornea bank (Beverwijk, the Netherlands, donor "D", n = 1). This study was approved by the medical ethical committee (TCBio) of the UMCU as protocol 18-740, by the medical ethical committee of the MUMC+ under protocol METC 2021-2732 and by the ETB-BISLIFE donor bank and was in accordance with the Declaration of Helsinki and the Dutch law. As patient samples were anonymized, sex, gender, age, race and other information were not recorded and is not available either for the organoid lines derived downstream of some of these samples. Hence, the impact of these factors has not been assessed on derivation efficiency nor on potential conjunctival cell population differences.

Viruses

Herpes Simplex Virus 1 containing endogenously tagged VP16 capsid protein with tdTomato (HSV1-tdTomato) was a kind gift from Prashant Desai (Johns Hopkins University, Baltimore, MD).[52] An hAdV8 strain isolated from a patient was provided by Dr. Nobuyo Yawata and Dr. Makoto Yawata (Kyushu University, Japan and NUS, Singapore).[54] Previously reported ancestral SARS-CoV-2 (614G, isolate BavPat1/2020 EVAg Ref-SKU: 026V-03883) and the Delta variant (GenBank accession number: OM287123) were

used in this study. Biosafety level 2 (BSL-2) infections were conducted at the Hubrecht Institute following Dutch regulations. The use of genetically modified HSV1 virus was performed under license IG 17-262. All work with infectious SARS-CoV-2 was performed in a Class II Biosafety Cabinet under BSL-3 conditions at Erasmus Medical Center, following the Dutch regulations.

METHODS DETAILS

Mouse organoids

Conjunctiva of surplus WT C57/BL6 female mice was dissected out and minced using a scalpel. No microdissection to remove the fibroblast layer was performed. The tissue suspension was incubated with 0.5% Trypsin-EDTA (ThermoFisher scientific) diluted 1:1 in Advanced DMEM/F12 (Gibco, final concentration 0.25%) for 10–15 minutes in a water bath at 37°C. The tissue suspension was vigorously pipetted up and down using a P1000 pipette every 5 minutes. Digestion was stopped when small epithelial fragments and/or single cells were obtained by adding 10 mL of Advanced DMEM/F12 (ThermoFisher scientific). Cells were then pelleted at 500 × *g* for 5 minutes, washed a second time with 10 mL Advanced DMEM/F12 (ThermoFisher scientific) and pelleted again. The pellet was resuspended in about 100 μL per eye of Cultrex Pathclear Reduced Growth Factor Basement Membrane Extract (BME, 3533-001, Amsbio). BME was allowed to solidify for 25–30 minutes at 37°C before adding expansion medium. Mouse expansion medium consisted in: Advanced DMEM/F12, 10 mmol/L HEPES (11560496, ThermoFisher scientific), GlutaMAX (11574466, ThermoFisher scientific), 100 U/mL Penicillin-Streptomycin (11548876, ThermoFisher scientific) [hereafter called AdDMEM+++], B27 Supplement (1X, 11530536, ThermoFisher scientific), 1.25 mM N-acetylcysteine (A9165, Sigma-Aldrich), 0.25% Noggin conditioned medium (U-Protein Express), 5% R-spondin 1 conditioned medium (produced as described in Pleguezuelos-Manzano et al[89]), 50 ng/ml EGF (AF-100-15, Peprotech), 100 ng/mL FGF1 (Peprotech), 3 μM A83-01 (2939, Tocris), 10 μM ROCK inhibitor Y-27632 (M1817, Abmole) and 100 mg/mL Primocin (ant-pm-1, Invivogen). Organoids were maintained in a humidified 37°C incubator with 5% CO_2. Every 7-10 days, organoids were dissociated to single cells using 0.5% Trypsin-EDTA (Gibco) diluted 1:1 in AdDMEM+++ similarly to organoid establishment and plated at a 1:6-1:8 ratio. When required, mouse expansion medium was changed for mouse differentiation medium 10 days after splitting. Mouse differentiation medium consisted in: AdDMEM+++, 1.25 mM N-acetylcysteine (A9165, Sigma-Aldrich), 0.25% Noggin conditioned medium (U-Protein Express), 5% R-spondin 1 conditioned medium (produced as described in Pleguezuelos-Manzano et al[89]), 3 μM A83-01 (2939, Tocris), 10 μM ROCK inhibitor Y-27632 (M1817, Abmole) and 100 mg/mL Primocin (ant-pm-1, Invivogen). Mouse conjunctiva organoids were kept in differentiation medium for up to 9 days.

Human organoids

Conjunctival samples of about 1 mm^3 were kept cold in AdDMEM+++ supplemented with 100 mg/mL Primocin (ant-pm-1, Invivogen) until further processing (< 4 hours). In the lab, human conjunctival samples were digested exactly like mouse samples. When needed, part of the sample was fixed for histological analyses (see after). The cell pellet was resuspended in BME and human expansion medium was added upon BME solidification. Human expansion medium consisted of mouse expansion medium supplemented with 0.15 nM Wnt Surrogate (U-Protein Express), 100 ng/mL FGF10 (100-26, Peprotech) and 1 μM Forskolin (1099, Tocris). As EGF was reducing the life span of the organoids (passage number), it was removed from the medium. Only single-cell mRNA sequencing of the organoids under expansion and differentiation was performed on organoids cultured in EGF-containing medium. Human conjunctival organoids were split every 10 days similarly to their mouse counterparts and plated at a 1:4 ratio. When needed, expansion medium was replaced for differentiation medium 10 days after splitting. Human differentiation medium consisted in AdDMEM+++, 1.25 mM N-acetylcysteine (A9165, Sigma-Aldrich), 0.25% Noggin conditioned medium (U-Protein Express), 5% R-spondin 1 conditioned medium (produced as described in Pleguezuelos-Manzano et al[89]), 3 μM A83-01 (2939, Tocris) and 10 μM ROCK inhibitor Y-27632 (M1817, Abmole). Human conjunctiva organoids were kept in differentiation medium for up to 11 days.

Growth factor withdrawal

Fresh mouse or human tissue were obtained, dissociated and plated as described above. The samples were divided by the number of conditions to be tested, ensuring the same number of cells were plated across all conditions. For each condition, a single growth factor was removed or added to the cells. For mouse organoids, exposure to human conjunctiva medium and to mouse lacrimal gland medium[81] was additionally performed. Organoid initial outgrowth was determined based on CellTiter-Glo 3D (Promega, G9683) following the manufacturer's recommendations. The luminescence readouts were normalized to the mouse or human conjunctiva medium control. Long-term growth of the organoids was assessed by repeated passaging of the organoid lines in the different conditions, which was performed as described above.

Air-liquid interface cultures

Human organoids (5–7 days after split) were harvested, trypsinized to single cells using 0.25% Trypsin/EDTA (ThermoFisher Scientific) for 5 minutes and 100,000 cells were seeded in 100 μL human expansion medium on 6.5 mm-wide transwells (Greiner) previously coated with rat tail collagen I (ThermoFisher Scientific). Human expansion medium was added to the lower compartment. After 3 to 4 days, when cells had reached confluency, medium from the upper compartment was removed to lift the cultures to air-liquid interface (ALI). The ALI cultures were maintained up to 22 days. The medium in the bottom compartment was changed every 3-4 days. When indicated, the ALI cultures were exposed to 5 ng/mL interleukin 4 (Peprotech, 200-04), 5 ng/mL interleukin 13 (Peprotech,

200-13) and 10 μM DAPT (Sigma Aldrich, D5942) from the moment medium was removed from the upper chamber. Air-liquid interface culture was performed with similar outcomes for 10 lines, with passage numbers varying from 1 to 14.

RT-qPCR analysis of gene expression

RNA was extracted from organoids contained in 100 μL of BME, from ALI cultures or primary tissue using the RNeasy Mini Kit (-QIAGEN) and resuspended in 25 μL nuclease-free water (QIAGEN). Reverse transcription was performed on at least 500 ng RNA per condition with GoScript Reverse Transcriptase (A5003, Promega) and Random primers (C1181, Promega) according to the manufacturer's instructions. Quantitative PCR was performed with SYBR green (1725270, Bio-Rad) on a CFX384 Touch Real-Time PCR detection system (Bio-Rad). Primers are listed in Table S7.

Histology

Tissue was fixed in formalin for at least 2 hours. Organoids were dissociated from the BME by washing with 10 mL ice-cold AdDMEM+++ per 100 μL BME, followed by pelleting at 300 × *g* for 5 minutes. Then, organoids and ALI cultures were also fixed in formalin for at least 2 hours. At that stage, the transwell membrane with cells on it was cut out from the transwell insert and further processed. Tissue, organoids and transwells were finally embedded in paraffin by performing serial incubations in EtOH 70%, EtOH 96%, EtOH 100%, Xylene and liquid paraffin. 4 μm-sections were made, hydrated, and subjected to hematoxylin and eosin (H&E) and PAS staining as described before,[17] and/or to immunohistochemistry. For immunohistochemistry, antigen retrieval was performed according to the respective antibody manufacturer's instructions. Then, sections were blocked with 1% Bovine Serum Albumin (BSA, MP Biomedicals, 160069) in PBS. For staining, the following antibodies were used: TP63 (ab735, Abcam), PAX6 (Biolegend, 901301), KI67 (eBiosciences, 14-5698-82), mouse KI67 (abcam, ab16667), human KI67 (BD Pharmingen, 550609), MUC5AC (ThermoFisher Scientific, MA5-12175), MUC1 (Abcam, ab15481), AQP5 (Origene, TA307525), LCN2 (R&D systems, AF1757), WFDC2 (LSBio, LS-C175346), mouse KRT19 (Cell Signalling Technology, 13092S), human KRT19 (Cell Signalling Technology, 4558S), AVIL (Sigma-Aldrich, HPA058864), SLC4A4 (Atlas Antibodies, HPA035628) and TFF3 (Atlas Antibodies, HPA035464). After overnight staining with the primary antibody at 4°C, sections were washed 3 times with PBS. If needed, sections were incubated with a secondary antibody rabbit anti-goat (Southern Biotech, 6160-01) for 1 hour and washed 3 times with PBS. Lastly, sections were incubated for one hour with BrightVision poly-HRT anti-rabbit (Agilent, K400311-2) or BrightVision poly-HRT anti-mouse (Agilent, K400111-2) and with 3,3'-diaminobenzidine (DAB) for 10 minutes. Finally, sections were dehydrated and mounted using Pertex®. Sections were imaged using a DM4000 optical microscope (Leica). Images were processed using the ImageJ software (FIJI).

Immunofluorescence

First, organoids were retrieved from BME as described above. Organoids and ALI were fixed in formalin for 2–24 hours, permeabilized for 20 minutes in 0.2% Triton-X and blocked using 1% BSA and 0.2% Triton-X. Overnight staining was performed at 4°C with one of the above-mentioned antibodies or anti-adenovirus hexon proteinlip) or anti-SARS-CoV nucleoprotein in 1% BSA and 0.2% Triton-X. Organoids and ALI were then washed 3 times in PBS and stained for one hour in the dark at room temperature while rotating with the appropriate secondary antibody: Alexa Fluor 488 donkey anti-rabbit (Thermo Fisher Scientific, A21206), Alexa Fluor 568 donkey anti-mouse (Thermo Fisher Scientific, A10037), Alexa Fluor 568 donkey anti-rabbit (Thermo Fisher Scientific, A10042) or Alexa Fluor 568 donkey anti-goat (Thermo Fisher Scientific, A11057). In some cases, Phalloidin–Atto 647N (Sigma-Aldrich, 65906) and DAPI (Sigma) were added to the mixture. After 3 washes of PBS and 1 wash of MilliQ, organoids and ALI on the transwell membrane were mounted in Prolong Gold antifade reagent with DAPI (P36935, Thermo Fisher Scientific) on a slide. Slides were imaged using either an SP8 or an SP8X confocal microscope (both Leica). Images were processed using ImageJ (FIJI).

CRISPR/Cas9-mediated knock-out of *Pax6*

About 5 days after splitting (when the organoids were in the growth phase), they were dissociated into near single cell similar as for passaging. Half a plate of mouse organoids at passage 16 was taken per gene to knock-out (~ 600 μL BME). The cell suspension was washed and pelleted at 500 × *g* for 5 minutes. Then, organoids were resuspended in 80 μL BTXpress solution (45-0805, BTX) supplemented with 100 μM ROCK inhibitor Y-27632 (M1817, Abmole). 10 μg of pSpCas9(BB)-2A-GFP containing Pax6 gRNA (Pax6_gRNA_F: CACCgCTCTACGATCTTCTGCCGGG and Pax6_gRNA_R: AAACCCCGGCAGAAGATCGTAGAGc) cloned as previously described,[90] 7.2 μg of hygromycin resistance containing transposon and 2.8 μg of transposase[105] were added to the cell suspension. The suspension was transferred to an electroporation cuvette right before electroporation. Electroporation was performed with NEPA21 using settings of a previous publication.[106] Immediately after, 400 μL of BTXpress supplemented with Y-27632 was added to electroporated cells and the cells were allowed to recover at room temperature for 30 minutes before plating. Importantly, a control without hygromycin transposon and transposase was also electroporated. This served as a selection control later on. After recovery, cells for Pax6 gRNA and control cells were plated at a similar density and expansion medium was added. When organoids had recovered from the electroporation and started to grow (about 3-5 days after electroporating), selection with Hygromycin (1:1000, Invivogen) was initiated. When all control cells had died (within < 5 days), surviving clones were picked, dissociated and clonally expanded. To check for *Pax6* deletion, DNA from the clones was extracted using 50 μL QuickExtract™ DNA Extraction Solution 1.0 (QE09050, Lucigen) and PCR-mediated genotyping of the clones was performed using the following primers: Pax6_gen_F TCCAGTGGGCAGGTTCAAAT and Pax6_gen_R AGGACGCTTAGAGTGGAGGGCC. Clones with out-of-frame deletions were kept for further analyses and organoids at passage 20 to 30 were used for downstream analyses.

Bulk mRNA sequencing

RNA was isolated from organoids, as done for qPCR analyses. Bulk mRNA sequencing was performed by Single Cell Discoveries (Utrecht, Netherlands). Briefly, polyA-enriched RNA was reverse transcribed and sequenced on an Illumina NextSeq500. For the mouse bulk sequencing, paired-end reads were mapped to the mouse (mm10) using the publicly available pipeline MapAndGo (https://github.com/vertesy/TheCorvinas/blob/102b598cc8e3717c155c5c5ea974488fe7992d96/Python/MapAndGo/) and the default settings for BWA-MEM. For the viral infection assay, reads were mapped to a human genome (hg38) using STAR (version 2.7.8a), reads with multiple mapping positions were excluded. Reads were associated with genes if they were mapped to an exon. Reads were collapsed into UMI tables using umi_tools (version 1.1.1). Analysis of bulk RNA-seq samples was performed in R. DESeq2 (version 1.26.0)[101] was used to perform differential expression analysis between infected and naïve samples. clusterProfiler (version 3.14.0)[103] and ChIPpeakAnno (version 3.20.0) were applied to perform gene functional annotation of differentially expressed genes. When comparing gene expression levels, all samples were down-sampled to the minimal depth (3.155 M transcripts per sample).

Pterygium samples analysis

Healthy conjunctiva and pterygium bulk mRNA sequencing samples were previously published[23] and retrieved from the GEO database (accession number: GSE155776). Differentially expressed genes between pterygium and healthy samples were identified using the GEO2R tool on the GEO, which uses DESeq2.

Sample preparation for single-cell mRNA sequencing

The following samples were subjected to single-cell mRNA sequencing: (1) human conjunctival organoids cultured in expansion medium for 5 days (donor M16 – palpebral – passage 5), (2) human conjunctival organoids cultured in expansion medium for 10 days and in differentiation medium for 7 days (donor M16 – palpebral – passage 4), (3) human conjunctival ALI when cells had just reached confluence (i.e. 3 days after seeding, named ALI day 0, from donor M16 – palpebral – passage 6), (4) human conjunctival ALI 3 days after shifting to air-liquid interface (donor M16 – palpebral – passage 5), (5) human conjunctival ALI 17 days after shifting to air-liquid interface (donor M16 – palpebral – passage 3, donor M16 – bulbar – passage 10), (6) human conjunctival ALI 15 days after shifting to air-liquid interface exposed to IL-4/-13 (donor M16 – bulbar – passage 4), and (7) human tissue from 4 pooled donors (all bulbar conjunctiva).

Tissue samples were obtained one month before the processing. At time of sampling, these were immediately minced in the operating room and placed in 1 mL of CellBanker 1 (Amsbio, 11888) on dry ice. The samples were stored at -80°C until further processing. On the day of the sort, the 4 biopsies were thawed, pooled and washed with 10 mL of AdDMEM+++.

To dissociate the samples, cells were resuspended in 1 mL of 0.25% Trypsin/EDTA (Gibco) and 10 U/mL DNase I (Sigma Aldrich, DN25) and incubated in a 37 °C water bath, while checking the advancement of dissociation regularly under the microscope. Using a pre-wet narrowed Pasteur pipette, the cell suspensions were mechanically dissociated by pipetting up and down. The cell suspensions were washed twice with AdDMEM+++.

The cell suspensions from 17 day-old ALI cultures were resuspended in 1 mL FACS buffer (PBS-MQ + 10% Fetal bovine serum - Sigma-Aldrich, F7524). The tissue cell suspension was treated for 5 minutes at RT with red blood cell lysis buffer (Sigma Aldrich, 11814389001), before being washed once with AdDMEM+++. Finally, the cell suspension was resuspended in 1 mL FACS buffer. The cell suspensions that were multiplexed (i.e. conditions 1, 2, 3, 4 and 6) were incubated in labelling oligos CMO303, CMO304, CMO305, CMO306 and CMO307, respectively, for 15 minutes at RT. Then, cells were washed with 6 mL FACS buffer and resuspended in 1 mL of FACS buffer.

Immediately before the sort, DAPI (ThermoFisher Scientific, D1306) and DRAQ5 (Biostatus, 62251) were added to the cell suspensions. Living cells (that is DAPI- and DRAQ5+) were sorted on a BD Jazz sorter (BD Bioscience) into FACS buffer. 30,000 cells were used for library preparation using the 10x Genomics Chromium 3' Gene Expression solution v3.1. The samples that were multiplexed were multiplexed in the ratios 1 (EM) : 2 (DM) : 1 (ALI day 0) : 1 (ALI day 3) : 5 (ALI day 15 + IL-4/-13). The libraries were sequenced on a NovaSeq6000 (Illumina).

Single-cell mRNA sequencing analysis

The reads were mapped to the human genome (hg38) and, when needed, demultiplexed using cellranger (v7.1.0). Reads from the tissue samples were demultiplexed based on SNPs using Souporcell.[100] Intronic reads were included in the count matrices. Tissue cells had a median of 18,714 reads and 2,680 genes per cell. ALI day 17 (donor M16) had a median of 27,933 reads and 3,436 genes per cell. ALI day 17 (donor M16) sample had a median of 31,236 reads and 3,613 genes per cell. ALI day 0 sample had a median of 14,298 reads and 2,702 genes per cell. ALI day 3 sample had a median of 9,205 reads and 2,143 genes per cell. ALI day 15 + IL-4/-13 sample had a median of 12,984 reads and 2,725 genes per cell. Organoids in EM had a median of 17,761 reads and 3,143 genes per cell. Organoids in DM had a median of 14,555 reads and 2,672 genes per cell.

Transcript counts from the different conditions were loaded in the Seurat package v3 and v4.[96] Unassigned cells and doublets identified by CellRanger or Souporcell were excluded before downstream analysis. Cells with fewer than 10 % mitochondrial reads and genes comprised between 500 and 7,500 were retained. The datasets were normalized and the top 3,000 variable features were identified in each. Then, the datasets scaled and integrated with *rpca* reduction using 3,000 integration features, following the Seurat vignette. The uniform manifold approximation and projection (UMAP) projection and the nearest-neighbors graph calculation were

performed using the first 40 dimensions. Clustering was performed with resolution 0.7. Cell types were identified based on the expression of marker genes and the clusters were renamed accordingly. Differential expression analysis was performed on the renamed clusters to obtain the gene expression signature of each cell type. GO term enrichment analyses were performed using the goseq package.[102]

To identify the effect of IL-4/-13 treatment on the transcriptome of each cell type, the ALI day 17 and ALI day 15 + IL-4/-13 samples were subset from the initial dataset. Then, differentially expressed genes were calculated in each cell type upon treatment.

To perform subclustering analysis, the goblet cells, tuft cells, and basal cells were subset from the original dataset. For goblet and tuft cells, the 3000 most variable features were identified based on the RNA assay of the Seurat object. These features were used to scale the integrated assay, before clustering using the first 15 dimensions and a resolution of 0.5 for goblet cells and 1 for tuft cells. For basal cells, the subset object was re-clustered without rescaling using 15 dimensions and a resolution of 1.

To compare conjunctival goblet cells to other tissue goblet cells, we first retrieved human lung,[91] gut[92] and stomach[93] atlases from previous publications. From the gut atlas, epithelial cells from healthy individual were retained and down-sampled (500 cells per cell type, based on published annotations). We down-sampled the lung atlas to 200 cells per cell type based on the published annotations. For the stomach atlas, we re-analyzed all healthy samples to identify cell types, especially goblet cells. For this, we retained cells with < 10% mitochondrial reads and 500 < genes per cell < 7500. The datasets were normalized, the top 2,000 most variable features were identified, the datasets were scaled and integrated using 2,000 integration features. Then, the integrated stomach dataset was clustered based on the 10 first dimensions and with a resolution of 0.5. Stomach goblet cells were identified based on the expression of *MUC2*. Then, the dataset was down-sampled to 500 cells per cluster. The stomach, lung, gut and conjunctiva down-sampled datasets were then loaded into Seurat v4. These were merged, normalized and scaled based on the 2,000 most variable features. Following UMAP embedding, the differentially expressed genes between the goblet cells from the conjunctiva, the colon, the small intestine, the lung and the stomach were identified. Then, the Pearson correlation between the gene expression profiles of each tissue goblet cell population was calculated.

Single-cell organoid outgrowth

Human conjunctival organoids cultured in expansion medium for 7–11 days were dissociated into single-cells as described above. Cells were counted and stained with 5 μL per 10^6 cells of PE anti-human NGFR (345106, Biolegend) for 30 minutes at 4°C in the dark. Cells were then washed, resuspended in human expansion medium and strained (35 μm). DAPI was added immediately before the sort. 1000 living cells (DAPI-negative) NGFR-positive and NGFR-negative were sorted into human expansion medium, pelleted and plated in 20 μL BME to follow organoid outgrowth. Pictures were taken on a brightfield Leica microscope and an AutoEvos (Thermo Fisher Scientific). The number of organoids growing out per condition was counted manually using ImageJ (FIJI) after 6 days. Single-cell clones were further expanded and subjected to histological analyses.

Supernatant collection

24 hours before harvest, the upper compartment ALI cultures were washed with 100 μL of PBS to remove any previously secreted material. Then, 50 μL PBS was added on the apical surface of the ALI and the ALI was allowed to secrete products for 24 hours later, after which the supernatant was collected, spun down at 10,000 × *g* for 5 minutes to remove cell debris, and frozen down until further processing. The same process was repeated at the indicated time points on the same ALI culture. For Western Blot and Dot Blot, the total volume of the supernatant was normalized with PBS to the maximum volume across all samples.

Western blot

For mouse organoid Western Blot, Pax6 WT and KO organoids were removed from the BME by a 30 minute incubation in 0.125 U/mL dispase (17105-041, ThermoFisher Scientific) at 37°C. The pellet was washed and resuspended in RIPA buffer (50 mL Tris-HCl pH8, 150 mM NaCl, 0.1% SDS, 0.5% Na-Deoxycholate, 1% NP40, 1x complete protease inhibitors (Roche)). The protein concentration per sample was measured using Micro BCA™ Protein Assay Kit (ThermoFisher Scientific) and adjusted.

For human ALI Western Blot, the collected supernatants were mixed with Laemmli buffer containing 100 mM DTT (Sigma) and boiled for 5 minutes. After spinning, supernatants were collected.

The samples were loaded on a 4–15% gradient gel (4561083, Bio-Rad) and run at 100 V for 1 hour. Proteins were transferred onto a nitrocellulose membrane with ice blocks at 100 V for 1 hour. The membrane was blocked using 1% BSA in TBST (TBS containing 0.1% Tween (Sigma Aldrich)) and stained overnight using primary in 1% BSA in TBST. The next day, membranes were washed 3 times with TBST and incubated with secondary antibody for 1 hour in blocking buffer. After 3 washes with TBST, the membranes were incubated in ECL detection reagent (ThermoFisher Scientific, 12393969) following the manufacturer's instructions. Membranes were imaged on an ImageQuant LAS 4000 ECL (GE Healthcare Life Sciences). The following antibodies were used: LCN2 (R&D systems, AF1757), PAX6 (Biolegend, 90131), GAPDH (Labned, LN2100751), rabbit anti-goat HRP (Dako, P0449), swine anti-rabbit HRP (Dako, P021702-2) and rabbit anti-mouse HRP (Dako, P0161).

Dot blot

2 μL of the collected supernatants (normalized for volume across conditions) were loaded directly on a nitrocellulose membrane and were allowed to dry for 5 minutes before blocking, staining, washing and revealing as explained above. The membrane was first stained for MUC5AC (ThermoFisher Scientific, MA5-12175) and rabbit anti-mouse HRP (Dako, P0161).

Secretome sample preparation

Secreted protein products were diluted to a final concentration of 8 M urea with 50 mM ammonium bicarbonate (pH 8, Sigma Aldrich), reduced in 10 mM dithiothreitol (DTT) at 20°C for 60 min, and alkylated in the dark with 20 mM iodoacetamide (IAA) at 20°C for 30 min. An additional final concentration of 10 mM DTT was added to quench the excess IAA. 50 mM ammonium bicarbonate was used to dilute to reach a final concentration of 2 M Urea. The alkylated proteins were sequentially digested using Lys-C (Wako, 129-05061) and trypsin (Sigma Aldrich) at a 1:75 enzyme-to-protein ratio, and carried out at 37°C. The Lys-C digestion lasted for 4 hours, and the trypsin digestion was performed overnight. 3% formic acid was used to quench the digestion, and digested peptides were desalted by Sep-Pak C18 1 cc Vac cartridges (Waters), dried using a vacuum centrifuge, and stored at -80°C for further LC-MS/MS analyses.

LC–MS/MS analyses

The secretome measurement was performed on an Orbitrap Eclipse Tribrid Mass Spectrometer (Thermo Fisher Scientific) coupled with a Vanquish™ Neo UHPLC System (Thermo Fisher Scientific) in data-dependent acquisition mode. Samples were analyzed in triplicates and separated on an analytical column (2 μm C18, 75 μm X 500 mm, Thermo Fisher Scientific) with a 175-min gradient. Peptides were first eluted at a constant flow rate of 300 nl/min using 0 to 32% solvent B (0.1% v/v formic acid in 80% acetonitrile) over 160 min, raised to 50% over 8 min, then ramped to 100% in 30 s and held for 6.5 min with a flow rate of 400 nl/min. Electrospray ionization was performed at a 2.1 kV static spray voltage; the temperature of the ion transfer tube was set to 275°C, and the RF lens voltage was set to 55%. Full scan MS spectra from the m/z range of 375-1600 were acquired at a resolution of 60,000 after accumulating to the 'Standard' pre-set automated gain control (AGC) target. Higher energy collision dissociation (HCD) was performed with 35% normalized collision energy (NCE), at an orbitrap resolution of 30,000. Dynamic exclusion time was set to 90 s and a 0.7 m/z isolation window was used for fragmentation.

Database search and analysis

Data search was performed using MaxQuant (version 2.4.2.0) with an integrated Andromeda search engine, against the UniProt human protein database (Downloaded on April 10th, 2023, containing 20,422 reviewed sequences) concatenated with the top 35 fetal bovine serum (FBS) contaminants. Digestion was defined as Trypsin/P and a maximum of 2 missed cleavages were allowed. Cysteine carbamidomethylation was set as a fixed modification, and protein N-terminal acetylation and methionine oxidation were set as variable modifications. Label-free quantification (LFQ) and the match-between-runs feature were enabled for protein quantification. A false discovery rate (FDR) of 1% was applied to both peptide spectrum matches (PSMs) and protein identification using a target-decoy approach. For total proteome measurements, intensity-based absolute quantification (iBAQ) was enabled.

Quantitative data filtering was conducted using the Perseus software (version 1.6.15.0). Proteins that cross-matching to bovine contaminants were removed along with potential contaminants, reverse peptides, and proteins only identified by sites. LFQ intensities were log_2-transformed. One replicate originating from donor M4 from removed from the analyses owing to the low number of proteins detected in expansion medium, pointing at a technical issue. Proteins that were quantifiable in at least two out of three replicates were retained. Imputation was performed based on the normal distribution. Secreted protein annotation was manually curated against UniProt Knowledgebase annotation. Data was plotted with R version 4.1.0.

Herpes Simplex Virus 1 infection

For HSV1 infection of 17-day-old ALI cultures, HSV1-tdTomato virus was added apically to the ALI (in the transwell) in 50 μL PBS at an MOI of 0.1 for 3 hours. After 3 hours, the supernatant was removed and the transwell was washed 2 times with 150 μL PBS. Then, every 24 hour, the secreted virus was collected in 100 μL PBS (including at 0 hour post-infection). In brief, PBS was added to the transwell, pipetted up and down 3 times and collected after 15 minutes. The collected supernatant was then stored at -20°C until further processing. If indicated, 10 μM acyclovir (PHR1254, Sigma-Aldrich) was added to the bottom compartment after incubating with the virus. In addition, ALI cultures were imaged daily to monitor viral progression using an Auto-EVOS microscope (Thermo Fisher Scientific). Viral titer quantification was performed as indicated below.

hAdV8 infection

Similar to HSV1 infection, hAdV8 at MOI 10 was added to the ALI culture in 50 μL PBS for 3 hours, before being washed away. Every 24 hours, the shed viruses were collected in 100 μL PBS and stored until further processing. If indicated, 10 μM acyclovir (PHR1254, Sigma-Aldrich), 60 μM cidofovir (C5874, Sigma-Aldrich) or 20 μM nelfinavir (PZ0013, Sigma-Aldrich) was added to the bottom compartment after incubating with the virus. hAdV8-infected ALI cultures were kept for up to 4 days and, if required, fixed.

Determination of the viral titers by qPCR

At the time of processing of the pellets for organoids and supernatants for ALI cultures, DNA was extracted using Quick-DNA Microprep kit (ZY-D3020, Zymogen). DNA was systematically resuspended in 15 μL nuclease-free water (QIAGEN). Viral DNA was then quantified by qPCR as follow: 5 μL of the DNA extract was mixed together with 5 μL of SYBR green (Bio-Rad) containing HSV1 or hAdV8 detection primers (Table S7). The SYBR green was mixed with 10 μM primer mix at a ratio 10:1. Technical duplicates were assessed by qPCR. The following program was used for viral DNA amplification: 95°C for 2 minutes,

followed by 40 cycles of 98°C for 15 seconds, 60°C for 15 seconds and 72°C for 15 seconds. For quantifying the viral DNA content in ALI supernatants, we amplified 179 bp of HSV1-tdTomato genome using HSV1-F and HSV1-R and 1004 bp of the hAdV8 genome using hAdV8-F and hAdV8-R. We cloned both in a pJet vector (Thermo Fisher Scientific) and used it to make a standard curve ranging from 2.10^4 to 2.10^9 copies of viral genome according to Addgene instructions (https://www.addgene.org/protocols/aav-titration-qpcr-using-sybr-green-technology/). Using this standard curve, we deduced how many viral genome copies were shed in the supernatant. Infection experiments were always conducted in technical triplicates and repeated in different organoid lines.

SARS-CoV-2 production

Calu-3 cells were maintained in Opti-MEM I (1X) + GlutaMAX (Thermo Fisher scientific), supplemented with 10% fetal calf serum, penicillin (100 IU/mL) and streptomycin (100 IU/mL) at 37°C in a humidified CO_2 incubator. Ancestral SARS-CoV-2 (614G, isolate BavPat1/2020 EVAg Ref-SKU: 026V-03883) and the Delta variant (GenBank accession number: OM287123) were propagated on Calu-3 cells in AdDMEM+++, and sequence confirmed as described before.[107] Virus titrations were performed by plaque assay.[108] All work with infectious SARS-CoV-2 was performed in a Class II Biosafety Cabinet under BSL-3 conditions at Erasmus Medical Center.

SARS-CoV-2 infection

For SARS-CoV-2 infections of 17 to 30-day old ALI cultures, expansion medium was refreshed and cultures were washed twice with 200 μL AdDMEM+++ before inoculation from the apical side at a MOI of 0.1 in 200 μL AdDMEM+++ per well. Next, cells were incubated at 37°C and 5% CO_2 for 2 hours before washing the apical side 3 times in 200 μL AdDMEM+++. At the indicated timepoints, virus was collected from the cells by adding 200 μL AdDMEM+++ apically, incubating 10 minutes at 37°C with 5% CO_2, and storing the supernatant at -80°C. Prior to determining the virus titer, samples were centrifuged at 500 × *g* for 5 minutes. Infectious virus titers were determined using by qRT-PCR using primers E_Sarbeco_F, E_Sarbeco_R and E_Sarbeco_Probe[94,109] (Table S7), and by plaque assay on Calu-3 cells.[108]

Fixed immunofluorescence microscopy of SARS-CoV-2-infected 2D cultures

Cells were fixed in formalin, permeabilized in 70% ethanol, and blocked for 60 minutes in 10% normal goat serum in PBS (blocking buffer). Cells were incubated with primary antibody (Rabbit-anti-SARS-CoV NP, Sino Biological; 1:1000) overnight at 4°C in blocking buffer, washed with PBS, incubated with Alexa488-coupled secondary antibody (1:1000; Invitrogen) in blocking buffer for 2 hours at room temperature, washed with PBS, incubated for 20 minutes with Hoechst, incubated for 20 minutes in CruzFluor647-labeled phalloidin (Santa Cruz), washed with PBS, and mounted in Prolong Antifade (Invitrogen) mounting medium. Samples were imaged on an LSM700 confocal microscope using ZEN software (Zeiss).

Transmission electron microscopy

Fresh tissue and ALI samples were fixed in fixation buffer (2% paraformaldehyde, 2.5% glutaraldehyde in 0.1 M phosphate buffer at pH 7.4) for 24 hours at 4°C. Then, samples were kept in wash buffer (0.1 M cacodylate) until further processing. Samples underwent an additional fixation with 1% osmium tetroxide and 1.5% potassium ferricyanide in wash buffer for 1 hour in the dark at 4°C. Further, the samples were dehydrated in EtOH 100% and infiltrated with Epon resin for 2 days. Then, samples were embedded in Epon resin, which polymerized for 2 days at 60°C. Ultrathin sections were cut using an ultramicrotome (Leica Ultracut UCT) and mounted on Formvar-coated copper grids. Sections were stained with 2% uranyl acetate in water and lead citrate. Sections were imaged using a Tecnai T12 electron microscope and an Eagle 4k*4k CCD camera (Thermo Fisher Scientific).

Orthotopic transplantations in mouse

Human bulbar conjunctiva organoids were expanded as described above and split 4-5 days before the transplantation day. On the transplantation day, organoids were freed from BME using dispase as described before.[81] Organoids in their growth phase were resuspended in fibrin component 2 (TISSEEL, Baxter) and kept on ice until transplantation in mice. Immunodeficient NSG mice were sedated by intra-peritoneal injection of midazolam (10 μL/g body weight). Under a surgical microscope, the bottom bulbar conjunctiva of the right eye was excised using surgical scissors on an area smaller than 1 mm^2. Then, 5 μL of organoid suspension in fibrin component 2 (~ 100,000 cells) was placed on top of the wound. ~5 μL of fibrin component 1 was immediately added to induce fibrin polymerization. After the fibrin had polymerized, one drop of Fucithalmic ointment was added on the eye to prevent bacterial infections. The eyelids were stitched together to avoid blinking-related failure of the transplantation. To prevent pain, mice were injected with 0,1 mg/kg of buprenorphine on the day of the surgery and were provided with 0.06 mg/mL of carprofen in the drinking water for 2 days. Mice were sacrificed using CO_2 inhalation 2 days and 3 weeks after the surgery to assess organoid engraftment. The entire eye was dissected, fixed, and embedded in paraffin. Screening for engraftment of KRT19+ human cells or human nucleoli was performed histologically as described before.[81] When human cells were detected, consecutive sections were stained for conjunctival markers including TP63, MUC1 and KI67. To quantify the number of cells engrafted per engraftment site (i.e. clone), the number of nuclei positive for the human nucleolar marker were counted in two consecutive sections and averaged out.

QUANTIFICATION AND STATISTICAL ANALYSIS

Across figures, error bars indicate standard error to the mean. Unless otherwise stated, (paired) Student's tests were performed with hypothesis of variance equality only when this was verified. Statistical analyses and plots were done in GraphPad Prism v9 or R v4.1.0. The meaning of individual data points is specified in the figure legends.